Master Thesis

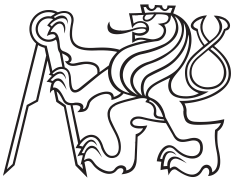

Czech Technical University in Prague

F3

Faculty of Electrical Engineering
Department of Computer Science

Analysis and classification of the subthalamic nucleus from microelectrode recordings

Minh Thao Nguyenová

Supervisor: Ing. Eduard Bakštein, Ph.D.
Field of study: Medical Electronics and Bioinformatics
Subfield: Bioinformatics
August 2021

"This is the void. We call it void not because we know it is empty but because we do not know what it is full of."

- Nathan W. Pyle

Acknowledgements

First of all, I would like to thank Ing. Eduard Bakštein, Ph. D. for introducing me to the world of neuroinformatics, patiently supervising this thesis, and guiding me through the whole process. Additionally, my thanks belong to Mgr. Tomáš Sieger, Ph. D. for helpful suggestions, consultations, and invaluable insight into the problematics. Especially, my gratitude goes to my family for making me who I am, being there for me whenever I needed, and the amazing homemade meals, because for us, food is an equivalent of love. And to Jakub, for always washing the dishes, his endless patience, support, and everything else.

Declaration

Prohlašuji, že jsem předloženou práci vypracovala samostatně, a že jsem uvedla veškerou použitou literaturu.

V Praze, 13. srpna 2021

Abstract

Deep brain stimulation is a commonly employed treatment of advanced Parkinson's disease. It is based on stimulating deep brain structures, also known as basal ganglia, with high-frequency electric pulses through a stimulation electrode, which is permanently implanted in the brain. Prior to the stimulation electrode implantation, invasive microelectrode mapping of the potential stimulation area is taken. These measurements record the electrophysiology of the nearby neurons to ensure correct stimulation targeting. The signals measured during such exploration are called microelectrode recordings and are the subject of analysis in this thesis. Subthalamic nucleus is a typical target of deep brain stimulation in Parkinson's disease treatment. This thesis approaches to classify this structure from the microelectrode recordings. Besides, the neural oscillatory activity of the basal ganglia in the beta frequency band (13 - 30 Hz) is extracted from the microelectrode recordings. The beta activity is then studied in relation to its localization in the basal ganglia and the clinical symptoms of Parkinson's disease.

Keywords: Parkinson's disease, Deep Brain Stimulation, subthalamic nucleus, microelectrode recordings, micro-EEG, μEEG, beta activity, electrophysiology, neural activity

Supervisor: Ing. Eduard Bakštein, Ph.D.
Analysis and Interpretation of Biomedical Data, FEE

Abstrakt

Hluboká mozková stimulace je často aplikovanou léčbou v pokročilých stadiích Parkinsonovy choroby. Její princip je založen na stimulaci hlubokých mozkových struktur, také známých jako bazální ganglia, vysokofrekvenčními pulzy přes permanentně implantovanou stimulační elektrodu. Před její samotnou implantací se provádí invazivní mapování potenciální stimulační oblasti pomocí mikroelektrod. Tato měření zaznamenávají elektrofyziologii okolních neuronů a zajišťují správné zacílení stimulace. Signály naměřené během takové explorace se nazývají mikroelektrodové záznamy a jsou předmětem analýzy v této práci. Subthalamické jádro je typickým cílem hluboké mozkové stimulace v léčbě Parkinsonovy choroby. Tato práce se zabývá klasifikací subthalamického jádra s mikroelektrodových záznamů. Kromě toho jsou z dat extrahovány neurální oscilace bazálních ganglií v beta frekvenčním pásmu (13 - 30 Hz). Tato beta aktivita je poté studována ve spojitosti s lokalizací mikroelektrodových záznamů v rámci bazálních ganglií a klinickými symptomy Parkinsovovy choroby.

Klíčová slova: Parkinsonova choroba, hluboká mozková stimulace, subthalamické jádro, mikroelektrodové záznamy, mikro-EEG, μEEG, beta aktivita, electrofyziologie, neurální aktivita

Překlad názvu: Analýza a klasifikace subthalamického jádra z mikroelektrodových záznamů

Contents

Figures

Tables

Chapter 1

Introduction

Contemporary methods in medicine have brought tremendous progress in terms of understanding the human body, its organ systems, their functions, and the interconnections between them. Using a broad range of measurement tools, it is possible to identify various types of deviations to recognize pathologies, their origin, expression, and progress. Each measurement brings specific data and a unique view on the system state and actions. Despite such advances, the brain and neural structures remain mostly undiscovered. The human brain is a complex organ built of the order of 10^{10} neurons, which are interconnected with each other through synapses. Each neuron communicates with thousands of other neurons [Silbernagl and Despopoulos, 2008]. It is therefore beyond the possibilities of current science to fully understand the complete brain structure and related processes.

In the past decades, various conditions related to aberrations of brain structure were studied. Parkinson's disease (PD), which affects 1% of the world population above 60 years, is one of the most prevalent among them. The cardinal symptoms of Parkinson's disease are related to motor skills, namely, tremor, rigidity, and bradykinesia. Occurrence of these symptoms was found to be related to the degradation of dopaminergic neurons in the brain. The lack of dopamine then disturbs the exhibition-inhibition balance in the motor regulation pathways in the basal ganglia causing motor impairment [Armstrong and Okun, 2020]. Despite the fact that the cause of the neural death is yet not completely understood and there is no cure to revert or stop their deterioration, dramatic advances were made to relieve the symptoms, which considerably ameliorate patients' quality of life. A common treatment method for advanced PD motor symptoms is deep brain stimulation (DBS), first introduced in 1987 [Gardner, 2013]. Since then, the treatment has been largely optimized for efficiency while mitigating the stimulation side effects. DBS is based on stimulating a target structure in the basal ganglia, typically the subthalamic nucleus (STN), with high-frequency electric pulses. Due to the size and location of the STN, the stimulation electrode placement is a very complicated and delicate task. The current approach in most centres combines 3D medical imaging methods with invasive microelectrode measurements for precise electrode implantation. The microelectrodes are inserted along the planned implantation trajectory and map the surrounding neural activity. The measurements are called microelectrode recordings (MER), microrecordings, or micro-EEG (μEEG). Such signals present not only a tool for deep brain structure localization, but also a unique insight into their *in vivo* electrophysiology. This information is invaluable as deep brain structures are otherwise hardly accessible with less invasive methods.

This thesis aims to process the clinical MER data and interpret their features in relation to their clinical relevance and stimulation electrode targeting. The main goals are specified as follows. Firstly, to contribute to the microelectrode recording (MER) dataset by acquiring, converting, and preprocessing new clinical data. Secondly, to implement a classifier for the subthalamic nucleus identification from clinical MER data and verify its performance on the prepared dataset. Although the neurosurgeons are trained to identify the STN through audiovisual signal inspection, automatic STN classification provides an objective support to the surgeon's decisions. We base our classifier on the signal normalized root mean square (NRMS) feature introduced by [Moran et al., 2006], which has been positively evaluated in literature [Konicarová, 2021]. In addition to that, we analyze the clinical MER spectral features inside and outside the STN with focus on activity in the beta band (13 - 30 Hz). The beta activity contribution to STN classification is then evaluated. Thirdly, we implement a visualization tool for the MER signals in our dataset and its attributes to facilitate data inspection and provide an idea of the feature distribution in 3D space. And finally, we identify the sensorimotor region of the STN and the neural beta oscillations. These two attributes are supposed to be closely related according to literature, where sensorimotor region of STN coincides with elevated beta activity observed in local field potential (LFP) measurements. Several approaches of beta activity recognition are taken and compared, as the beta activity feature is not generally specified and each resource authors propose a different method [Zaidel et al., 2010], [Contarino et al., 2012], [Horn et al., 2017], [van Wijk et al., 2017], [Tinkhauser et al., 2017], [Koirala et al., 2020]. Our clinical MER data have different characteristics and limitations than LFP data, which puts additional challenges on beta activity identification. To verify our methods, the results on the clinical data are compared to the beta activity observed in nonfiltered broadband MER signals, which correspond to the main source of data for beta activity analysis in the relevant literature. An additional clinical interpretation of the beta activity is the relation to the PD symptoms severity, which is also evaluated in this thesis.

The structure is organized as follows. The necessary medical background to the problem is explained in Chapter 2 along with the origin of the analyzed data. We describe the methods used throughout the work in Chapter 3. The results of the applied methods in several tasks given in the assignment are reported in Chapter 4. Our findings are then discussed in Chapter 5 in context of existing research. Finally, Chapter 6 concludes the whole thesis, summarizing its contributions and potential future work.

Chapter 2

Background

This chapter aims to provide a basic insight into the source of the signals further analysed in this thesis. It introduces the necessary medical background, including a brief description of symptoms, origin and current understanding of Parkinson's disease (PD) in Section 2.1. Contemporary methods of treatment are characterized in Section 2.2 and further with an emphasis on deep brain stimulation (DBS) in Section 2.3. Afterwards, Section 2.4 elaborates on the subthalamic nucleus (STN), a common target area of DBS, its anatomy, and other characteristics. The electrophysiological activity of a single neuron is briefly covered in Section 2.5. Section 2.6 reviews spectral features of the analysed electrophysiological signals with special attention to beta band (13-30 Hz) activity. Finally, Section 2.7 introduces Unified Parkinson's disease rating scale, a widely used tool of PD severity assessment, and its subsets handled in this thesis.

2.1 Parkinson's disease

Parkinson's disease is the second most common (after Alzheimer's disease) neurodegenerative disorder. It originates in the neural system and has an irreversible progressive character. The nerve cells in the deep brain structures gradually degrade, which cause the symptoms to worsen over time. Unfortunately, contemporary medicine has no cure for PD, which could revert or stop the deterioration of nerve cells. However, there are methods to relieve the main PD symptoms. If applied appropriately, they dramatically increase the quality of the patient's life and may slow down the disease progression.

The main symptoms of Parkinson's disease affect motor skills. There are five primary motor symptoms, which disturb the patient's movement in general: akinesia, bradykinesia, rigidity, tremor, and postural instability [Moustafa et al., 2016]. Akinesia is defined as a difficulty initiating movements and a poverty of action. Bradykinesia is characterized by a slowness of movement. It is closely related to and often examined together with akinesia. Rigidity is described as a stiffness experienced by the patient during voluntary movements. It can be also expressed as a stiffness during passive limb stretching done by the examiner. As for tremor, there are several types. Rest tremor is the most common in PD, while action and postural tremor occur mostly in other disorders, such as essential tremor disorder [Bhidayasiri, 2005]. The secondary motor symptoms are built upon primary symptoms and movement coordination difficulties. They are associated with impairment of complex motor behaviors, such as walking gait, speech, handwriting, and facial expression [Moustafa et al., 2016].

Besides motor symptoms, nonmotor symptoms may also appear and affect many organ systems. They include loss of smell, sleep dysfunction, such as daytime sleepiness or rapid eye movement sleep behavior disorder, or gastrointestinal and genitourinary difficulties, possibly leading to autonomic dysfunction. These symptoms, although not PD specific, occur in early stages and may allow to diagnose or predict PD before the characteristic motor symptoms develop [Chaudhuri et al., 2010]. Hallucinations and cognitive impairment affecting attention, executive, and visuospatial functions are associated with advanced PD [Armstrong and Okun, 2020].

As already mentioned, Parkinson's disease is a disorder caused by irreversible deterioration of nerve cells. According to the hypothesis published by [Braak et al., 2003], the pathophysiology of PD starts in the brainstem with lesions in the medulla oblongata and pontine tegmentum. In this initial stage, nonmotor symptoms appear, often not taken into consideration as potential PD symptoms [Chaudhuri et al., 2010]. As the disease progresses, the degeneration of nerve cells extends to areas of the midbrain, specifically the substantia nigra pars reticulata (SNr), which contains the nerve cells responsible for the production of dopamine hormone. Death of dopaminergic neurons and the resulting lack of dopamine leads to insufficient regulation of neural pathways in the deep brain structures (basal ganglia), followed by motor impairment, which is characteristic for PD. Therefore, PD is typically diagnosed at this stage [Armstrong and Okun, 2020]. Later on, the pathology spreads to the mesocortex and allocortex. In advanced PD, the neocortex is involved, specifically the sensory association and premotor areas, causing cognitive impairment, dementia, and hallucinations [Braak et al., 2003].

2.2 Treatment

The treatment of PD is symptomatic, as there is currently no cure to resolve the underlying pathophysiology and stop the disease progression. Early stage treatment is usually pharmacologic. Since the motor symptoms are caused by degradation of dopaminergic neurons and thus decreased dopamine level, the therapy aims to compensate it. The most common medications are levodopa preparations. Levodopa is a dopamine precursor, which metabolizes into dopamine in the basal ganglia, but also in other organ systems. Along with levodopa, other medications may be added to the therapy to enhance the dopamine release. Majority of patients respond well to medication with levodopa [Fox et al., 2018]. However, with the progression of the disease, patients require higher and more frequent doses due to progressive pathophysiological changes [Chou et al., 2018]. Such increased levodopa dosage is related to a higher risk of medication side effects caused by the dopamine level fluctuations, such as various gastrointestinal problems, dyskinesia, sudden recurrence of the motor symptoms, and functional disabilities between doses. There are also variants of PD appearing in 9-16% of patients, which are resistant to medication. For some of these cases, there are options for invasive therapy affecting directly the basal ganglia structures through neurosurgical methods. There are two neurosurgical approaches: lesional method based on burning out brain tissue in a particular target area, and deep brain stimulation (DBS), the latter being much more commonly used in recent years [Dallapiazza et al., 2018].

2.3 Deep Brain Stimulation

Deep Brain Stimulation (DBS) is a therapeutic method commonly used to alleviate otherwise treatment-resistant symptoms [Herrington et al., 2016]. In Parkinson's disease, it is used to alleviate the motor symptoms in patients with severe impairment and a sufficient response to previous levodopa medication. The stimulation target can be either the globus pallidus interna (GPi) or the subthalamic nucleus (STN). The choice of the target area depends on several indications, such as dominating symptoms or psychiatric anamnesis [Dallapiazza et al., 2018]. The stimulation can be either unilateral; i. e., solely in the right or left hemisphere, or more often bilateral; i. e. stimulating both nuclei. Besides PD, DBS is also used in therapy of chronic pain disorders, essential tremor, dystonia, obsessive-compulsive disorder, or chronic depression [Kringelbach et al., 2007]. Besides the deep brain structures, other areas of the brain might be also stimulated in neuropsychiatric therapy; for example, cortical stimulation in the treatment of epilepsy or schizophrenia.

DBS in PD is based on continuous stimulation of a target area in the basal ganglia with high-frequency (>130 Hz) electric pulses, which have been found empirically to be the most effective although the actual regulation mechanism remains unknown [Herrington et al., 2016]. The stimulation is provided by a neurostimulator, which is typically implanted in the chest cavity and generates the pulses applied to the target area through subcutaneous wiring and stimulation electrode implanted in deep brain structures. The stimulator also usually contains the reference electrode [Walckiers et al., 2010]. See Figure 2.1 for illustration of a typical DBS setup. During the implantation surgery, the patient's head is fixed in a stereotactic frame. A hole of approximately 14 mm in diameter is drilled in the skull and the electrode is inserted through a straight-line trajectory, which is carefully planned and calculated in advance using 3D imaging methods, usually magnetic resonance imaging (MRI) or computer tomography scans (CT) [Kringelbach et al., 2007]. The stimulation electrodes are of a long cylinder shape with 1.27 mm in diameter. The implantation of the electrode is done preferably with the patient awake, in order to observe the neural activity undistorted by anesthesia, and the immediate effects of brain tissue penetration.

Nevertheless, due to the small dimensions of basal ganglia; for instance, the maximum dimension of STN is approximately 8.5 mm, and the pliability of the brain issue, the actual position of the target area during surgery may differ significantly from the plan. Typical imaging methods are not sufficiently precise due to low resolution and potential target location alterations. Therefore, the electrophysiological activity is used in most centers as an additional indicator to distinguish particular deep brain structures [Israel and Burchiel, 2004]. Prior to the DBS electrode implantation, an invasive measurement (exploration) is performed, when the electrophysiological activity of surrounding neurons is measured and recorded. Recordings are made via electrodes with smaller dimensions than stimulation electrodes in order to cause as little damage to brain tissue as possible. Because of the electrode dimensions being as small as 5 μm in diameter, the recording electrodes are also called microelectrodes and recorded signals are referred to as micro-EEG (μEEG), microelectrode recordings (MER) or microrecordings. Such small electrode tip size allows to record the extracellular single-neuron activity and observe the individual action potentials (AP) (see Section 2.5 for explanation of AP). To make use of this feature, the recordings are sampled with frequency as high as 24 kHz. Thus, both spatial and temporal resolutions of MERs are significantly higher than is typical in other biomedical signals (electrocardiography, electroencephalography, etc.). The amplitude of the measured voltage ($\sim$ 1 mV) is also higher

than in conventional transcranial electroencephalography (EEG) ($\sim 10\mu$V) as a result of the invasive character of the measurement; i. e., measuring neural activity directly in the brain tissue [Israel and Burchiel, 2004]. For examples of typical measured signals, see Figure 2.2.

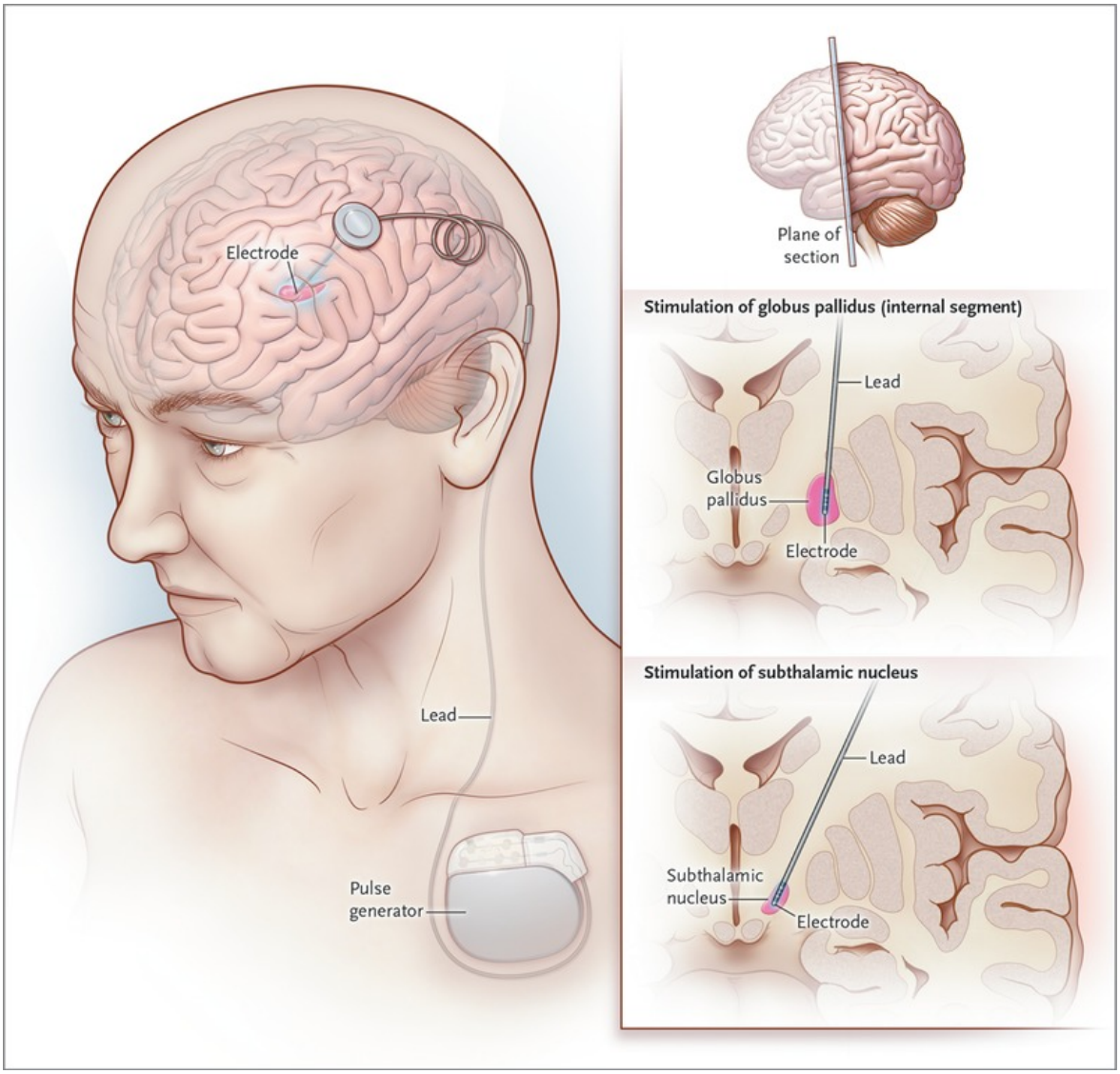

Figure 2.1: Deep brain stimulation setup illustration. Reproduced with permission from [Okun, 2012], Copyright Massachusetts Medical Society.

Throughout the operation, the acquired MER signals are filtered, amplified, and converted to an audio output. The surgeon is trained to recognize different areas in the basal ganglia during the exploration process according to the audio and visual signal inspection, see Figure 2.2 for illustration. The identified areas are then recorded in an operation protocol. According to these exploration findings, the surgeon decides where the stimulation electrode should be implanted for a successful treatment. Acquired recordings along with the operation protocol are then subject to further research for a better understanding of basal ganglia physiology. The technical process of MER acquisition and processing is described more thoroughly in Chapter 3.

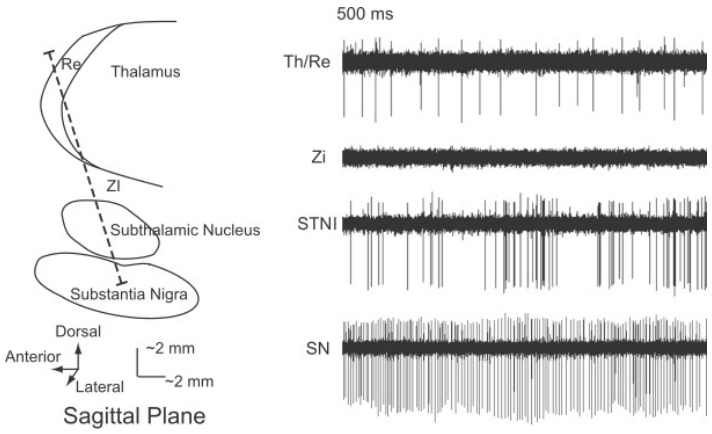

Figure 2.2: MER visual characteristics in different basal ganglia structures [Michmizos et al., 2017]. Copyright © 2017, IEEE.

2.4 Subthalamic nucleus

In this thesis, we focus on deep brain stimulation of the subthalamic nucleus, which is indicated as the target area for most Parkinson's disease patients with tremor dominant symptoms and no psychiatric disorder history [Dallapiazza et al., 2018]. Although rather small in size, STN is an integral part of various brain pathways. Besides motor, it also has an influence on associative functions and the limbic system; i. e., emotional and impulse control [Silbernagl and Despopoulos, 2008]. It is believed, that the anatomy of the nucleus is divided into regions according to these functions. The functional topography of primate STN is shown in Figure 2.3.

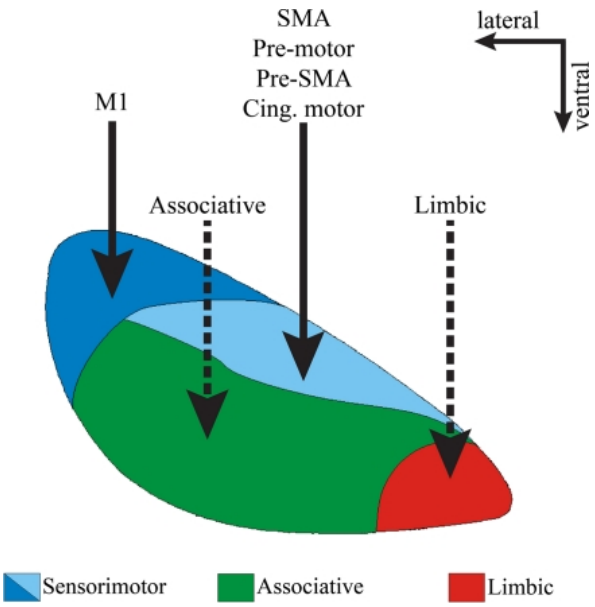

Figure 2.3: Topography of primate STN. Coronal view. [Mathai and Smith, 2011]. © 2011 Mathai and Smith.

Given the STN involvement in multiple regulation systems, the STN-DBS may also affect emotional, behavioral, or cognitive functions, depending on the electrode localization

within the STN. Sub-optimal stimulation placement increases the probability of postoperative development of addiction, depression, anxiety, or other neuropsychiatric disorder [Serranová et al., 2019]. To minimize the risk of such side effects, while maximising the therapeutic outcome, it is favorable to target not only STN itself, but also specific areas within [Akram et al., 2017]. The motor part of the STN is located on the dorsolateral end. Stimulation of this part was associated with better improvement of motor symptoms and lower risk of neuropsychiatric complications [Zaidel et al., 2010]. Such placement should lead to an efficient stimulation even with a smaller pulse amplitude. Identification of STN itself from microelectrode recordings has been achieved during the past decades using various signal features and probabilistic models [Moran et al., 2006], [Bakstein et al., 2016], [Konicarová, 2021]. Subregions of STN with different functions and stimulation effects have also been recognized by many authors [Zaidel et al., 2010], [Akram et al., 2017], [Horn et al., 2017], [Serranová et al., 2019], [Koirala et al., 2020], [Milosevic et al., 2020]. However, such task is complicated by the fact, that there are no clear boundaries of such areas, hence the objective ground truth to support the findings is missing.

2.5 Neural activity

The human nervous system is composed of more than 10^{10} nerve cells (neurons). The neuron is the structural and functional unit of the neural system [Silbernagl and Despopoulos, 2008]. It consists of the body (soma), a single axon, and multiple dendrites. Nerve cells are highly interconnected through dendrites, where the input stimuli are received, and axons, through which the output signal is transmitted to other neurons. The information is transmitted as an electrical signal produced by fluctuating concentrations of ions inside and outside the cell. The neuron membrane potential is defined as the difference between the inside and outside electric potentials. The resting potential of a neuron is the membrane potential during an electrochemical balance. It is usually around -70 mV. Despite the fact that the electric potential amplitude in principle changes its value continuously, the information produced by a neuron is rather of a discrete character. The neuron reacts to stimuli either by remaining silent or by creating an action potential (AP). This attribute is known as the All-or-None law [Silbernagl and Despopoulos, 2008].

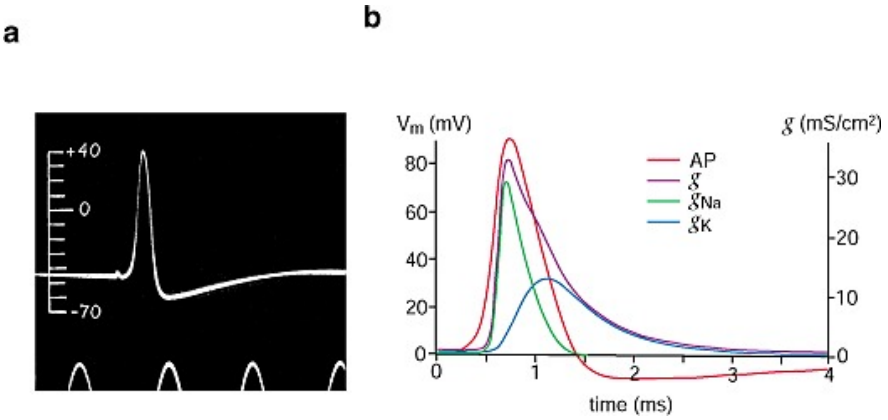

Figure 2.4: Action potential and fluctuating membrane conductance for different ions. Copyright © [Häusser, 2000]

An AP is a fast ($\sim$ 1 ms) peak of voltage with an amplitude significantly higher than the resting potential caused by sudden changes of cell membrane conductivity for certain ions, mostly Na^+ or K^+ (see Figure 2.4). The spike is followed by a refractory period, when the neuron remains silent. After the refractory period is over, the neuron may produce another AP depending on the input stimuli. Therefore, the output information of a neuron is coded in the spike timing and frequency rather than the immediate electric potential values. A series of AP and time intervals between them is often referred to as spiking or firing.

2.6 Beta activity

Exaggerated beta oscillatory activity (13-30 Hz) in the basal ganglia is commonly found in patients with Parkinson's disease [Tinkhauser et al., 2017]. Although the mechanism is not yet completely understood, the correlation between the spectral power on frequencies in the beta band and PD symptoms severity has been reviewed by several authors [Oswal et al., 2013], [Horn et al., 2017], [Tinkhauser et al., 2017], [Telkes et al., 2018]. It has been also found, that the neural synchronization in the beta band decreased after an acute levodopa medication dosage and was associated with higher voluntary movement velocity and higher voltage of agonist muscle activity [Chung et al., 2018]. Furthermore, electric stimulation of basal ganglia at frequencies in the beta band results in slowing of movement and worsening of Parkinsonian symptoms in tested subjects [Oswal et al., 2013]. Therefore, it is believed that beta activity is a potential physiomarker of pathological disruptions in neural pathways causing the motor symptoms of Parkinson's disease.

Investigating neural oscillations at beta band frequencies may help optimizing deep brain stimulation outcomes. As observed in [Zaidel et al., 2010], the neurons in subthalamic nucleus form a distinct dorsolateral oscillatory region. The location of this area overlaps with the sensorimotor subregion of STN mentioned in Section 2.4, which is also situated in the dorsolateral part of STN. Hence, beta band oscillations are thought to mark the optimal stimulation target in the STN to enhance the medication response for alleviation of PD motor symptoms [Zaidel et al., 2010], [Horn et al., 2017]. Apart from electrode targeting during surgery, beta activity analysis can be used to regulate a closed-loop DBS to ameliorate the treatment effects. Traditionally, the DBS is based on continuous high-frequency pulses, where parameters are set according to patients' subjective symptom perception [Kringelbach et al., 2007]. However, experiments in primate models have shown closed-loop DBS superiority to the open-loop system [Rosin et al., 2011].

Spectral features of basal ganglia activity have also been correlated with nonmotor symptoms of Parkinson's disease. For example, theta activity has been implicated in cognitive processing. Elevated theta activity (2-8 Hz) has been found in patients with the occurrence of impulse control disorders [Oswal et al., 2013]. Furthermore, alpha band (9-14 Hz) reactivity to emotional stimuli has been an important mark of depression symptoms of PD [Huebl et al., 2011]. However, such mechanisms are out of the scope of this thesis due to the work span and inaccessibility of appropriate data. Further in this work, we focus solely on analysing the beta activity in relation to the motor impairment in Parkinson's disease.

2.7 Unified Parkinson's disease rating scale

As noted in Section 2.1, Parkinson's disease is a disorder with many different symptoms. Occurrence of the symptoms is individual and varies among patients. There has therefore been a need to quantify PD severity to observe the disease progression, treatment effects, or patient's eligibility for DBS surgery. To evaluate the symptoms of Parkinson's disease quantitatively, the Unified Parkinson's disease rating scale (UPDRS) was designed [Goetz et al., 2008]. It is now a widely used tool to assess PD severity. The patient, their caregiver, or both of them fill out a questionnaire. They rate a wide set of symptoms on a scale from 0 to 4 according to impairment severity:

0. No impairment
1. Slight
2. Mild
3. Moderate
4. Severe.

Conditions affecting the PD symptoms must be also specified, i. e., before or after DBS surgery, whether the patient is on medication, minutes since the last medication dose, whether the stimulation is turned on or off. The questionnaire consists of four parts in total:

1. Non-Motor Aspects of Experiences of Daily Living (nM-EDL)
2. Motor Aspects of Experiences of Daily Living (M-EDL)
3. Motor Examination
4. Motor Complications.

In this thesis, we focus on Part III - Motor Examination, specifically the axial (one-sided) symptoms associated with tremor, rigidity, and bradykinesia, which are most correlated with beta activity according to literature [Oswal et al., 2013]. Each set of symptoms is evaluated separately for the left and the right side of the body. Tremor score in this thesis is a sum of three ratings:

- Upper Extremity Rest Tremor - the highest seen amplitude of trembling of the stretched arm in front of the body with palms down,
- Lower Extremity Rest Tremor - the highest seen amplitude of trembling of the leg at rest,
- Upper Extremity Action Tremor - the highest seen amplitude of hand trembling during slow finger-to-nose maneuvres.

Rigidity is tested in the neck and each limb. The patient remains passive while the examiner moves the tested body part to check for rigidity. If no rigidity is detected, the test is repeated, while the patient performs an action maneuver (tapping fingers, fist opening/closing, etc.) on the side not being tested. Symptoms regarded in the rigidity score in this thesis are:

- Upper Extremity Rigidity - rigidity in the major upper limb joints (wrist, elbow, shoulder),
- Lower Extremity Rigidity - rigidity in the major lower limb joints (ankle, knee, hip).

As for bradykinesia, there are several one-sided tests to check the movement slowness. The examiner shows the patient a specific movement and asks them to repeat the movement several times as largely and as fast as possible. The amplitude, speed, rhythm, and other dynamics of the movements are then observed and rated on the 0-4 scale. Symptoms regarded in the bradykinesia score in this thesis are:

- Finger Tapping - tapping the index finger on the thumb,
- Hand Movements - opening and closing the hand,
- Hand Pronation - the arm is extended in front of the body and the palm is turned up and down alternately,
- Toe Tapping - tapping the toes with heel on the ground.

Chapter 3

Methods

This chapter describes the characteristics of the analysed data and explains the methods fundamental for this thesis and the subject in general. First, the analysed microelectrode recordings (MER), their acquisition, and characteristics are described in Section 3.1. Section 3.2 explains the signal preprocessing prior to feature extraction depicted in Section 3.3. The visualization tools used and implemented within this thesis are described in Section 3.4. Additional methods related to the subthalamic nucleus task are outlined in Section 3.5. At last, the statistical evaluation methods are outlined in Section 3.6.

3.1 Microelectrode recordings

Signals used in this thesis were acquired through invasive measurements (explorations) of neural activity in the basal ganglia prior to implantation of the DBS electrode as previously described in Section 2.3. The measurements are made through five parallel tungsten microelectrodes in a cross formation (also called a 'Ben-gun' formation) with 2 mm spacing between the neighbour electrodes. The electrodes in the formation are further referred to as central, anterior, posterior, medial, and lateral according to their position with respect to the patient's principal axes as in Figure 3.1. The acquired signals are sampled at 24 kHz, amplified, and band-pass filtered at 500 Hz - 5 kHz through the Medtronic Lead Point system. This system also removes the 50 Hz powerline interference upon recording.

During the exploration, the electrodes are inserted in the brain from the anterio-dorso-lateral direction along a straight-line planned implantation trajectory. As the insertion proceeds, the electric activity of the surroundings is measured in each electrode and each increment of depth. The depths are labeled with the distance (in mm) from the expected target area position, which is labeled as T. Recordings acquired before the T depth was reached are labeled as negative; e. g., T-1.5 depth is 1.5 mm above (before) the expected area. Recordings acquired after the target depth was reached are labeled as positive; e. g., T+2.0 depth is 2.0 mm under (after) the expected area. The current measurements are instantly converted to audio output. The surgeon interprets the sound and marks the identified area in an operation protocol. The recording starts in T-10 depth and continues according to the surgeon's instructions so as to locate the desired area while minimising brain tissue damage.

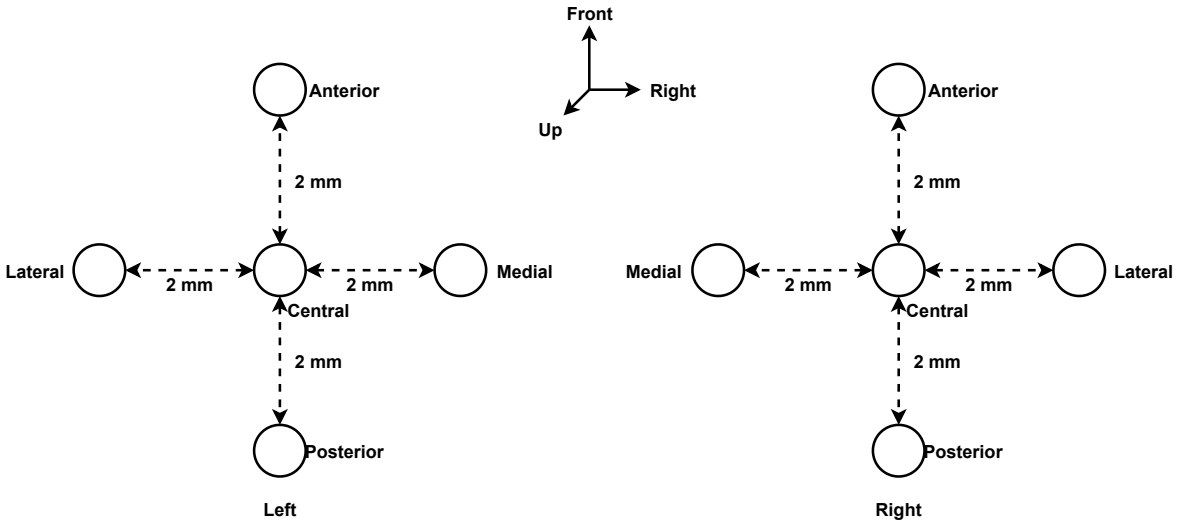

Figure 3.1: Ben-gun electrode formation schematic. Axial view.

Every patient's dataset contains a series of such recordings, each of 10s length, from every electrode and explored depth increment. The MER series is matched with the corresponding operation protocol scan (as in Figure 3.2), where the explored structures are labeled. After the DBS surgery, the MER data are extracted from the recording device, converted to binary format using LeadPoint proprietary software, anonymized, and finally imported into our dbsProcessing Data Access Object (DAO) developed by [Sieger, 2013]. Imported data are labeled according to the paired surgery protocols manually. This whole process must be done individually for each patient (twice in case of a bilateral implantation).

3.1.1 Broadband microelectrode recording

Due to the MER band-pass filtering in the recording setup, the background activity of the distant neural populations is mitigated in the clinical microelectrode recordings. Thus, the observed spectral features in the lower frequencies (<100 Hz) are very limited and mostly reflect the spiking activity of a few nearby neurons. In order to analyze the low frequency spectral features, an experimental recording setup made by BrainScope was added to the one already used for clinical purposes. The signals during the DBS surgery simultaneously with the clinical MERs using the same set of microelectrodes. These signals are high-pass filtered at 10 Hz and are otherwise not limited in frequency. Further in this thesis, such signals are referred to as broadband microelectrode recordings. Since 2016, the broad band MERs are recorded during experiments such as in [Serranová et al., 2019] in the Na Homolce hospital, Prague, Czech republic. Since 2020, the basal activity (at rest) is also recorded in the broadband signals along with the clinical ones.

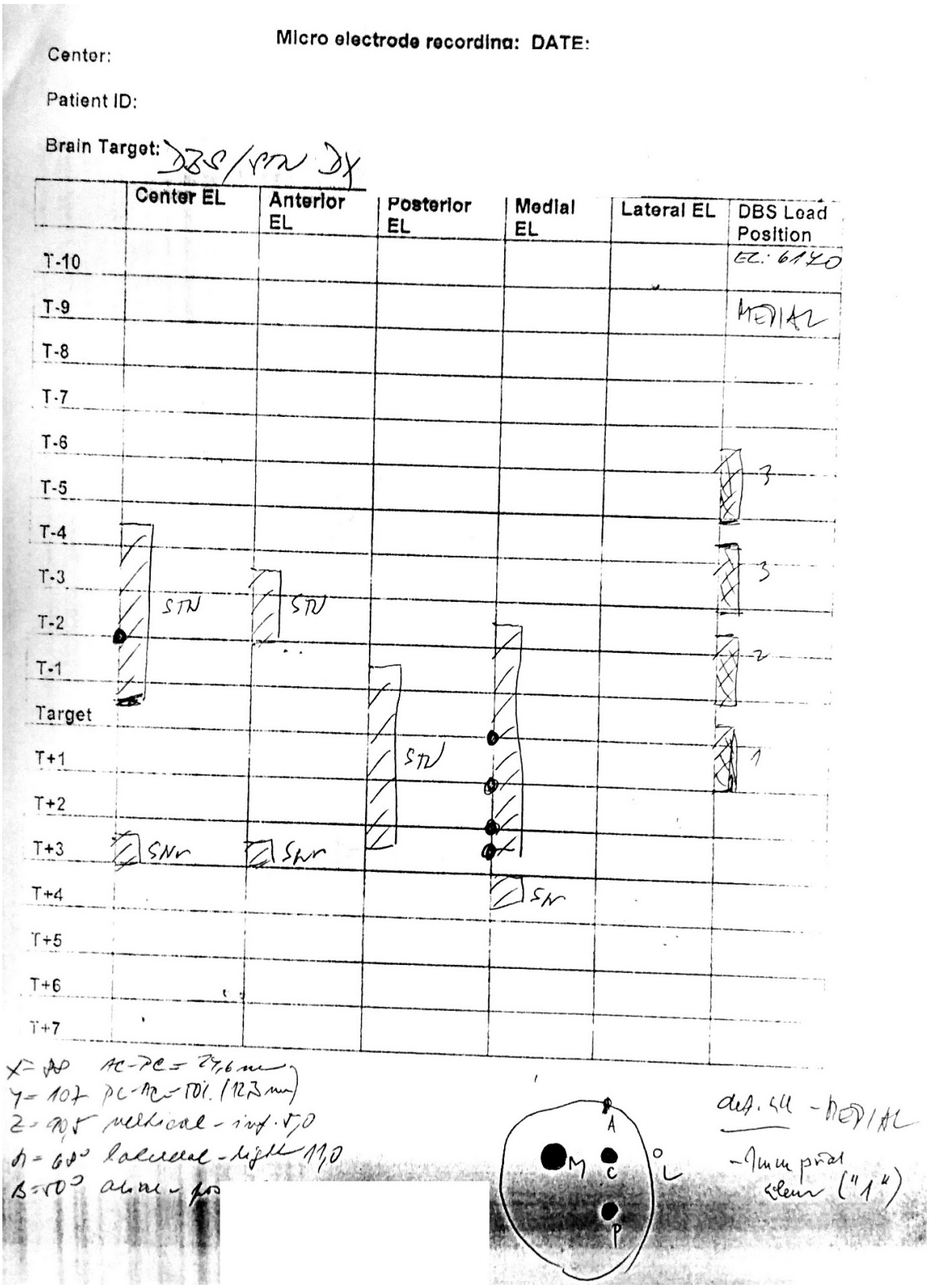

Figure 3.2: Example of an operation protocol.

3.2 Artifact removal

Given the small electrode tip size (∼1 μm) and low measured voltage (<1 mV), the MER signals are prone to gather various artifacts. Artifacts are a nonphysiological electric activity, usually caused by mechanical shifts or electromagnetic interference from the surrounding devices, which disrupts the information about the measured physiological activity. Despite preprocessing the signals upon recording, many artifacts remain in the data. Data disrupted with artifacts can be either removed manually, by visual inspection or using automatic detection methods. For the purpose of this thesis, we use a simple and straightforward method of maximum spectral difference as introduced in [Bakštein et al., 2017].

3.2.1 Maximum spectral difference

The main assumptions of this method are that the power spectral density (PSD) of an artifact-free band-pass filtered MER signal is smooth and its shape is similar across patients and electrodes, while the signals disrupted by artifacts commonly contain high peaks and other disturbances in their spectrum. At first, a model spectrum MP is calculated as the mean spectrum of the signal segments previously annotated as clean (artifact-free) by a team of professionals. Using a set of N training signals $T = \{X_1, X_2, ..., X_N\}$ and artifact annotations $A = \{y_1, y_2, ..., y_N\}$ with values $y_i = 1$ for a clean signal and $y_i = 0$ for a disrupted signal and P_i as the normalized PSD corresponding to the training signal X_i, the MP calculation can be described as

$$MP = \frac{1}{\sum_{i=1}^{N} a_i} \cdot \sum_{i=1}^{N} a_i \cdot P_i. \tag{3.1}$$

The normalized power spectral density P of a signal X is calculated dividing the original signal PSD by the total signal power. The sum of P is then always 1 and thus independent on the specific electrode impedance, which can vary significantly. The maximum spectral difference feature d for the assessed signal X is then calculated as the maximum absolute difference of its normalized spectrum P and the model spectrum MP over all M spectral bins as

$$d = \max_{m=1,...,M} |P(m) - MP(m)|. \tag{3.2}$$

The d value is then compared to a threshold to evaluate whether there is an artifact present. The threshold is optimized as in [Bakštein et al., 2017] on a separate training dataset. All spectra for MDP are calculated using Welch's method [Welch, 1967] (see Section 3.3.3) with Hamming window of 2048 samples (∼85.3s length, ∼11.72Hz resolution) and 50% window overlap. MER signals are divided into segments of 1s length. The d value is evaluated for each segment and the longest contiguous sequence of artifact-free segments is selected for further analysis and the rest of the recording is discarded.

3.3 Feature extraction

As can be seen in Figure 2.2, the MER signal has two compounds: the action potentials (spikes) of neurons close to the microelectrode and the background activity of remote neural

populations. To enhance the beta activity encoded as the firing frequency of nearby neurons, two different approaches are used. The first technique calculates the signal envelope from the analytic signal using Hilbert transformation. The other procedure converts the original signal into a binary signal with denoted times of neuron action potentials (spikes). Such signal is also referred to as a spiketrain. Effects of feature extraction methods on the spectrum calculation compared to using unprocessed signals are illustrated in Figure 3.3 on artificially generated signals.

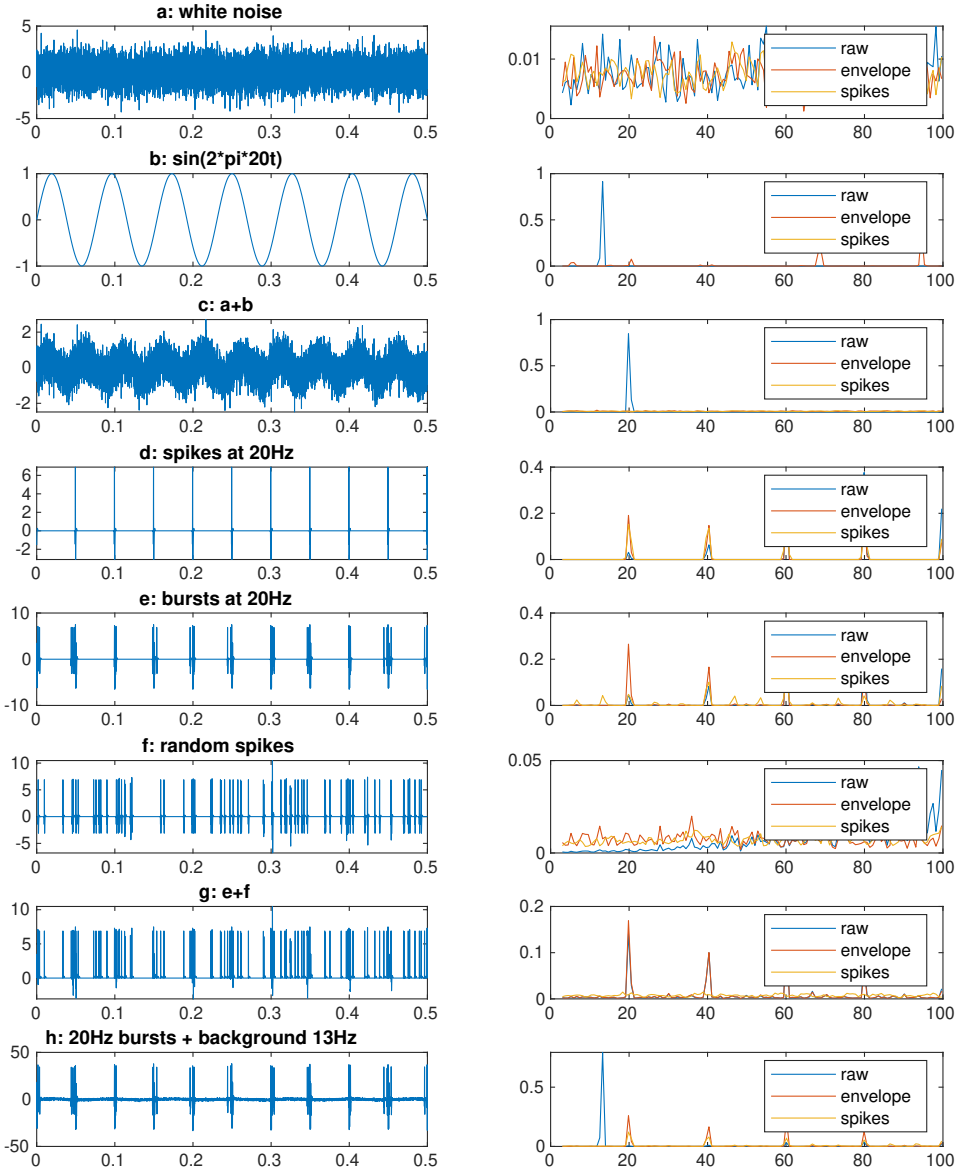

Figure 3.3: Demonstration of calculated PSD characteristics on synthetic signals.

3.3.1 Signal envelope

The main purpose of this method is to attain spiking activity in the signal with fast and simple tools. The signal envelope is calculated as the instantaneous amplitude of the signal, which is the absolute value of the corresponding analytic signal [Heil, 2007]. Analytic signal of a real-valued function $s(t)$ is defined as

$$s_a(t) = s(t) + j\hat{s}(t), \tag{3.3}$$

where j is the imaginary unit and $\hat{s}(t)$ is the Hilbert transform of $s(t)$. The Hilbert transform is defined as

$$H(u)(t) = \frac{1}{\pi} \text{ p. v.} \int_{-\infty}^{+\infty} \frac{u(\tau)}{t-\tau}, \tag{3.4}$$

where p. v. denotes the Cauchy principal value. An example MER segment illustrating the calculated signal envelope is in Figure 3.4.

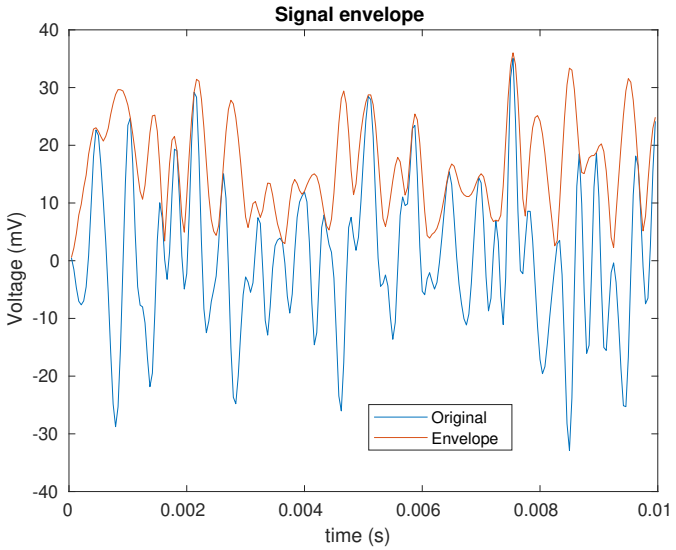

Figure 3.4: Example of MER signal envelope calculated from the analytic signal.

3.3.2 Spike sorting

As denoted in Section 2.5, information output of a neuron is encoded in the spiking times and frequency rather than the immediate voltage amplitude. Spike sorting process addresses this feature by detecting action potentials from the raw signal and assigning them to individual neurons surrounding the microelectrode. There are different approaches to spike sorting. In this thesis, we employ the WaveClus algorithm proposed in [Quian Quiroga and Nadasdy, 2004]. WaveClus has been reviewed on artificially generated noised data as the most accurate one in the comparison of three spike sorting algorithms made by [Wild et al., 2012],

The algorithm comprises the following steps. The first step is the spike detection. It consists of band-pass filtering to eliminate the background activity, followed by automatic amplitude thresholding. The threshold is calculated for each signal as a multiplied estimate of the standard deviation of the background noise σ_n.

$$Thr = 4\sigma_n; \quad \sigma_n = \text{median}\left\{\frac{|x|}{0.6745}\right\}, \tag{3.5}$$

where x is the band-pass filtered signal. In the second step, a small set of wavelet coefficients from each spike is chosen as an input for the clustering algorithm. Finally, the superparamagnetic clustering (SPC) classifies the spikes according to the selected set of wavelet coefficients. The main output of the spike sorting used in this thesis are spiketrains. A spiketrain is a binary signal with denoted times of detected action potentials belonging to one neural cluster.

3.3.3 Power spectral density

Power spectral density (PSD) for the artifact filtering and estimating beta activity was calculated using Welch's method [Welch, 1967], also known as the periodogram method. It is based on averaging periodograms calculated on partial signal segments. At first, the signal is sectioned into segments of a specified window length. The segments may overlap by a specified number of samples. Second, the segments are multiplied by a window function and the squared value of their discrete Fourier transform (DFT), also known as the periodogram, is calculated. And eventually the DFTs are averaged to form the overall power spectral density. The choice of the window type and length is derived from the demands on the PSD resolution and variance. A common choice is to set the number of samples in the window (window length) equivalent to the number of spectral bins in the resulting periodograms, as the maximum frequency resolution (spectral bin width) is equal to the window length inverse. Longer windows lead to higher frequency resolution, hence higher variance. Averaging higher number of periodograms enhances the robustness and thus reduces the PSD variance. In this work, we use the Hamming window of length 2048 samples (∼85 ms length, ∼11.72Hz resolution) in the artifact detection with maximum spectral difference, and 2^{15} samples (∼1.37 s length, ∼0.73Hz resolution) in the beta activity estimation. In both cases, the windows overlap by 50%.

3.3.4 Beta activity estimation methods

To calculate the beta oscillatory activity, the microrecordings were either used raw or adjusted using the methods described in Section 3.3. Afterwards, the PSD was calculated with Welch's method [Welch, 1967] using Hamming window with 2^{15} samples (∼1.37 s length, ∼ 0.73Hz resolution) and 50% window overlap. For analysis of spectral features, the PSD is then divided by the signal power to ensure independence on the electrode-specific impedance. The normalized spectra are further referred to according to the signals used for their calculation as:

- *raw* - from the raw (artifact-filtered) MER signal,
- *env* - from the analytic envelope of the MER signal,
- *spikesOne* - from the spiketrain of the neural cluster with the maximum amplitude extracted from the MER signal,
- *spikesAll* - from the unsorted spiketrain (including all neural clusters) extracted from the MER signal.

Finally, the beta activity was evaluated as either the maximum value (*-Max* methods) or the summed power (*-Sum* methods) in the 13-30 Hz beta band. Further in this thesis, the implemented methods of beta activity evaluation are referred to as:

- *rawMax* - maximum value in the 13-30Hz band of *raw* PSD,
- *envMax* - maximum value in the 13-30Hz band of *env* PSD,
- *spikesOneMax* - maximum value in the 13-30Hz band of *spikesOne* PSD,
- *spikesAllMax* - maximum value in the 13-30Hz band of *spikesAll* PSD,
- *rawSum* - summed power of the 13-30Hz band of *raw* PSD,
- *envSum* - summed power of the 13-30Hz band of *env* PSD,
- *spikesOneSum* - summed power of the 13-30Hz band of *spikesOne* PSD,
- *spikesAllSum* - summed power of the 13-30Hz band of *spikesAll* PSD,

3.4 Spectral features visualization

To facilitate visual inspection of a microelectrode recording (MER) dataset spectral features, two visualization tools were implemented within this thesis. They were also used for verification of exploration findings. The ProtocolPlot tool is an interactive MATLAB plot, where the signals are arranged in the same manner as the operation protocols in our dataset. The GUI-Beta3D tool is a MATLAB GUI application with the spectral activity shown in a Ben-gun 3D electrode spacing according to adjustable parameter settings. This section briefly describes the overall function of the tools. A more thorough documentation can be found in Appendix A.

3.4.1 ProtocolPlot

The ProtocolPlot tool displays the MER signal dataset of a single exploration along with the respective PSDs. The MER signals are filtered for artifacts and the longest contiguous clean segment is displayed and used for PSD calculation. Signals from each electrode are arranged in the respective columns. Each row corresponds to a certain depth position (distance from the estimated target), which is denoted in the leftmost column. Additional vertical lines in the PSD columns mark the frequency range of interest. The PSD is calculated using a subset of 4 available methods as listed in Section 3.3.4. The spectra are plotted in a grid along with the MER signals. In the grid plot, the PSDs are scaled to illustrate the spectrum characteristics, such as noisy spectrum, peaks at certain frequencies, or rising tendency towards high frequencies. The precise magnitudes can be viewed in the plots on the bottom, where the axes are labeled correctly according to the specific recording. Positions annotated as STN are marked with yellow background in the grid plot. The whole plot is interactive, it can be moved and zoomed as usual MATLAB plots. When clicking on a position area, the particular spectrum is plotted at the bottom left and the corresponding MER is plotted at the bottom right. An example of such visualization is shown in Figure 3.5.

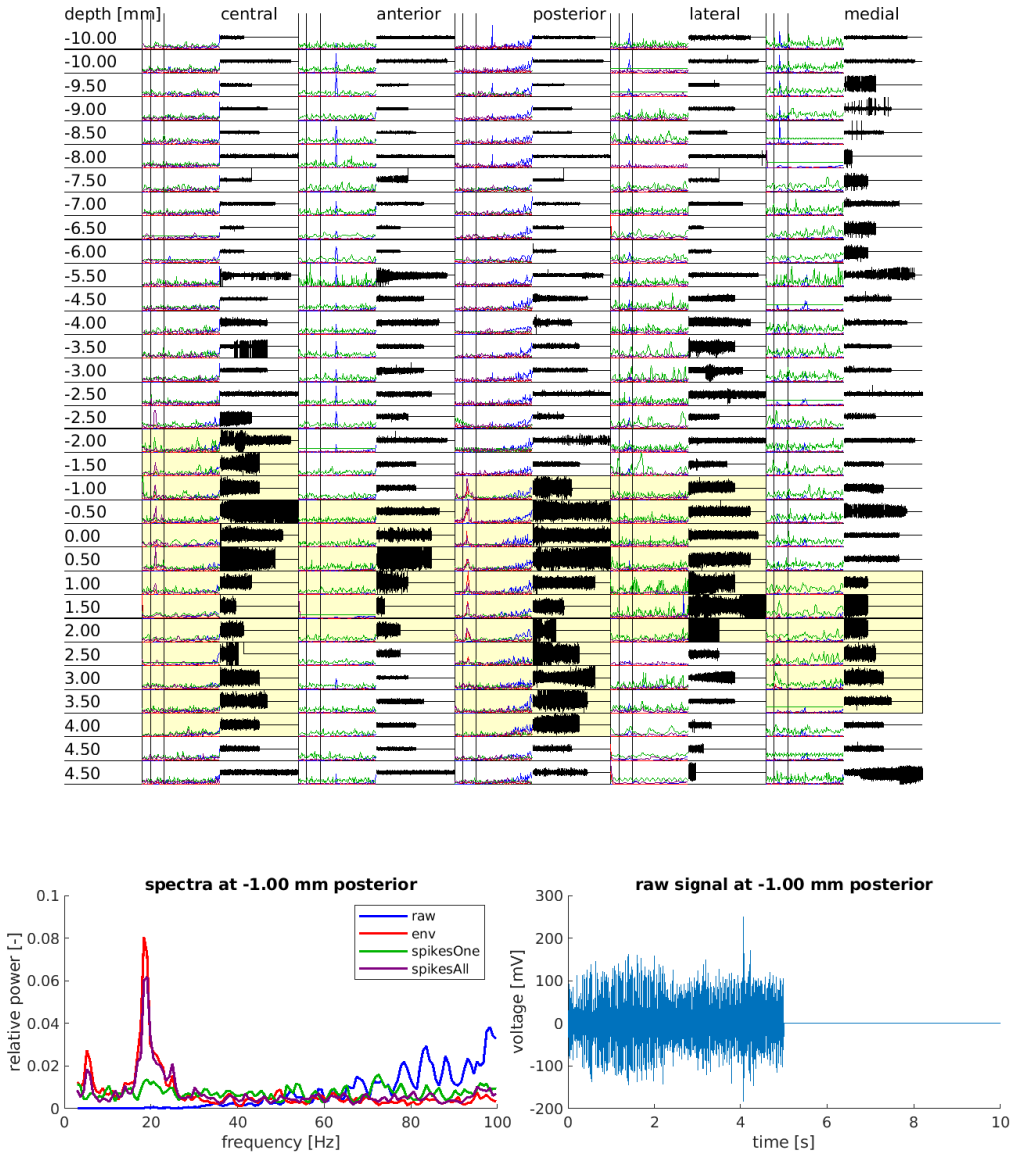

Figure 3.5: Exploration MER visualization using ProtocolPlot.

3.4.2 GUI - Beta3D

The GUI-Beta3D tool is a MATLAB application visualizing spectral features of MER data from an exploration in 3D electrode spacing. The application window is shown in Figure 3.6. The visualization is plotted in 3D axes on the left side of the window. The plot can be moved, rotated, or zoomed as usual MATLAB axes. It consists of five cylinders representing the electrode configuration. The X axis represents the front-back (anterior-posterior) electrode spacing and the Y axis represents left-right (lateral-medial for the left hemisphere, medial-lateral for the right hemisphere) electrode spacing. While the Z axis (cylinder height) represents the depth in which particular signals were recorded, the cylinder profile (diameter) shows the relative beta activity at the particular electrode and depth throughout the trajectory. Each cylinder segment is colored according to the specific area, where the MER was supposed to be acquired. The legend to the color labels is displayed on the right of the plot.

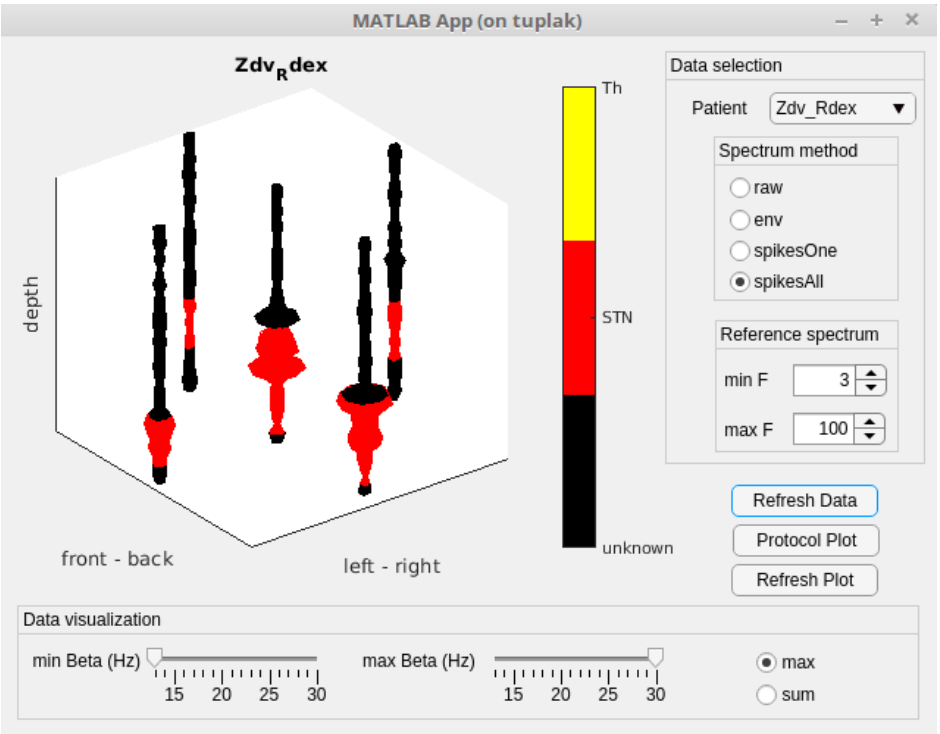

Figure 3.6: GUI-Beta3D application window.

The exploration dataset can be selected from the database in the dropdown menu in the top right corner. The parameters of the spectral features to be displayed can be adjusted using the control panels on the right and bottom of the application window. The parameter options and respective control panels are elaborated on in Appendix A.

3.5 Subthalamic nucleus classification

The final task of the assignment is to classify the subthalamic nucleus from microelectrode recordings. In the literature, there are many approaches to identify STN. According to comparison made by [Konicarová, 2021], the normalized root mean square (NRMS) of the signal is the most accurate from the evaluated selection and relatively simple and fast at the same time. Therefore, this method was chosen as the baseline approach to STN classification. The approach of STN classification using beta activity estimation was also tested. Afterwards, the contribution of beta activity evaluation to the NRMS-based STN classifier was studied through combining both approaches in a Support Vector Machine (SVM) classifier.

3.5.1 Normalized root mean square

The normalized root mean square (NRMS) value of a signal, originally suggested in [Moran et al., 2006], is the signal power normalized by a reference signal power, which is calculated for each trajectory and electrode from the first 5 measured positions, i. e., in depths from T-10 to T-8 in our dataset, which can be safely assumed to be prior to STN. The signal power or root mean square value (RMS) of signal $\mathbf{X}$ is calculated as

$$RMS(\mathbf{X}) = \sqrt{\sum_{i=1}^{n} \frac{x_i^2}{n}}, \tag{3.6}$$

where x_i is the $i-$th signal sample value and n is the length of signal $\mathbf{X}$. The reference signal power P_{ref} for a trajectory and electrode is calculated as a mean value of RMS at the first five positions p of the trajectory and electrode

$$P_{ref} = \sum_{p=1}^{5} \frac{RMS(\mathbf{X_i})}{5}. \tag{3.7}$$

The NRMS value of the signal is then calculated from RMS of the signal and the corresponding reference P_{ref} as

$$NRMS(X) = \frac{RMS(\mathbf{X})}{P_{ref}}. \tag{3.8}$$

The main advantage of the NRMS criterion is the length-invariance and impedance-invariance. Both of them are exploited in our case as the signal length varies due to artifact filtering, and the electrode impedance uncertainty stated by the manufacturer.

3.5.2 Support Vector Machine

Support Vector Machine (SVM) is one of the most popular machine learning concepts used for binary classification as it is simple, efficient, and well described in theory. This section contains a basic description of SVM principles as represented in [Mohri et al., 2012]. Training an SVM is defined as an optimization problem of finding a class-separating hyperplane. The general equation of a hyperplane in $\mathbb{R}^N$ is

$$\mathbf{w} \cdot \mathbf{x} + b = 0, \tag{3.9}$$

where $\mathbf{w} \in \mathbb{R}^N$ is a non-zero vector normal to the hyperplane, $\mathbf{x} \in \mathbb{R}^N$ is a point in space belonging to the hyperplane, and $b \geq 0$. The training point $\mathbf{x}_i \in \mathbb{R}^N$ with label $y_i \in \{-1, 1\}$ is correctly classified if

$$y_i = \text{sign}\left(\mathbf{w} \cdot \mathbf{x}_i + b\right). \tag{3.10}$$

In the case of separable data, the optimization problem can be formulated as a margin maximization problem. Margin ρ is the distance between the hyperplane and the closest member of the class. The margin maximization is equivalent to minimizing $||\mathbf{w}||$ or $\frac{1}{2}||\mathbf{w}||^2$. Thus, in the case of a separable dataset $T^m = \{(\mathbf{x}_1, y_1), ..., (\mathbf{x}_i, y_i), ..., (\mathbf{x}_m, y_m)\}$, the SVM solution can be defined as the solution to the convex optimization problem formulated as

$$\min_{\mathbf{w},b} \frac{1}{2}||\mathbf{w}||^2 \tag{3.11}$$

$$\text{s. t.:} \qquad y_i(\mathbf{w} \cdot \mathbf{x}_i + b) \geq 1, \quad \forall (\mathbf{x}_i, y_i) \in T^m.$$

However, in the case of an inseparable dataset T^m, for all hyperplanes, there exists such $(\mathbf{x}_i, y_i) \in T^m)$ that

$$y_i(\mathbf{w} \cdot \mathbf{x}_i) \ngeq 1. \tag{3.12}$$

Therefore, slack variables $\xi_i \geq 0$ are introduced to relax the conditions

$$y_i(\mathbf{w} \cdot \mathbf{x}_i) \ngeq 1 - \xi_i, \tag{3.13}$$

as ξ_i is the measurement of distance by which the constraint is violated. The slack variables are then added to the optimization as

$$\min_{\mathbf{w},\mathbf{b}} \frac{1}{2}||\mathbf{w}||^2 + C\sum_{i=1}^{m}\xi_i \tag{3.14}$$

$$\text{s. t.:} \qquad y_i(\mathbf{w}\cdot\mathbf{x}_i + b) \geq 1 - \xi_i \ \wedge \ \xi_i \geq 0, \quad \forall(\mathbf{x}_i, y_i) \in T^m,$$

where C parameter determines the trade-off between the margin maximization and minimization of the constraint violation penalty.

3.5.3 Hold-out validation

To provide an unbiased estimation of the classifier test error rate, it must be evaluated on previously unobserved data. In this thesis, such situation is modeled using hold-out validation strategy. The dataset is randomly split into three parts - the training, validation, and testing set. The model with a hyperparameter setting is fit on the training set and the fitted model is then used to predict the labels of the observations in the validation set. The optimal hyperparameter setting is chosen according to the results on the validation set. Finally, the fitted model with the chosen hyperparameter setting is used to predict the labels of the testing dataset, which provides an unbiased estimation of the classifier performance.

3.6 Statistical analysis methods

In order to evaluate our findings quantitatively, several statistical methods were used. Namely, a robust confidence interval calculation based on interquartile range, Wilcoxon paired rank-sum (Mann-Whitney U) test, Pearson correlation coefficient, and ROC curve. They are all described in this section as follows.

3.6.1 Confidence interval

The standard 95% confidence interval is an estimation of the range, where an observation should appear with 95% probability. It is calculated using the standard deviation (SD) around the mean value from n samples as

$$\left(\text{mean} - \frac{2\cdot SD}{\sqrt{n}}, \quad \text{mean} + \frac{2\cdot SD}{\sqrt{n}}\right). \tag{3.15}$$

However, due to the unknown SD and for better robustness to outliers, we decided to use the interquartile range (IQR) around the median value instead. In normal distribution, it is assumed that $IQR = 1.3 \cdot SD$. As a more conservative estimation, we assume that $IQR = SD$. Therefore, we calculate the 95% confidence interval around the median value using the interquartile range (IQR) from n observations as

$$\left(\text{median} - \frac{2\cdot IQR}{\sqrt{n}}, \quad \text{median} + \frac{2\cdot IQR}{\sqrt{n}}\right). \tag{3.16}$$

3.6.2 Wilcoxon rank-sum test

The Wilcoxon rank-sum test, also known as the Mann-Whitney U test, is used to make a comparison of two paired groups. One of the main advantages is that it is nonparametric, hence does not put any requirements on the population distribution. The only assumption is of randomly and independently chosen data samples. However, it has a lower statistical power, compared to its parametric counterpart (Student's t-test). The null hypothesis is that the two populations have the same continuous distribution. Values of each sample pair are compared. The number of "winning" samples, i. e., larger than its paired sample from the other group, is counted in each group. The smaller of the group sums, i. e., the resulting U statistic, is then consulted with significance tables. Generally, the more they differ, the more significant is the null hypothesis rejection. In this work, we use this method for comparison of beta activity on the front and back electrode in the motor subregion identification task.

3.6.3 Pearson correlation coefficient

Pearson correlation coefficient measures the linear correlation between two paired sets of data. Given sample set $S = \{(x_i, y_i),\ i \in [1, n])\}$ of size n, the correlation coefficient r_{xy} is calculated as

$$r_{xy} = \frac{\sum_{i=1}^{n}(x_i - \bar{x})(y_i - \bar{y})}{\sqrt{\sum_{i=1}^{n}(x_i - \bar{x})^2}\sqrt{\sum_{i=1}^{n}(y_i - \bar{y})^2}}, \tag{3.17}$$

where $\bar{x}$ and $\bar{y}$ are the means of the respective groups. The correlation coefficient is of value between -1 and 1. A large absolute value indicates a strong correlation between the groups, while correlation close to 0 indicates no linear relation in the data. An advantage of the Pearson correlation coefficient compared to the covariance measure is the normalization, which allows to indicate a relation between differently scaled data. However, it is limited by the linearity, hence nonlinear relations cannot be reflected in the coefficient. It is also not a robust measurement and thus prone to distortion caused by outliers. In this work, the investigated data correlations are between the criteria for STN classification, in comparison of clinical and broadband MER data, and between the identified beta activity and the PD symptoms severity.

3.6.4 P-value

In statistics, the P-value denotes the significance of the calculated result. It is defined as the probability of obtaining the same or more extreme results if the null hypothesis is valid. The null hypothesis can be rejected if the P-value is lower than the previously stated significance level [James et al., 2013]. In this thesis, we work with the most widely used 0.05 significance level. We evaluate the P-value of the Wilcoxon rank-sum test and the Pearson correlation coefficient.

3.6.5 Classifier performance

To evaluate a classifier performance on a dataset, the predictions are compared against the ground truth and the correct and incorrect classifications are counted as in Table 3.1

predictions \class member	Positive	Negative
Positive	True Positive (TP)	False Positive (FP)
Negative	False Negative (FN)	True Negative (TN)

Table 3.1: Contingency table.

The accuracy (ACC) of a binary classification is calculated as

$$ACC = \frac{TP + TN}{TP + FN + FP + TN}. \tag{3.18}$$

The true positive rate (TPR) or sensitivity of a binary classification is calculated as

$$TPR = \frac{TP}{TP + FN}. \tag{3.19}$$

The true negative rate (TNR) or specificity of a binary classification is calculated as

$$TNR = \frac{TN}{TN + FP}. \tag{3.20}$$

The false positive rate (FPR) of a binary classification is calculated as

$$FPR = \frac{FP}{FP + TN}. \tag{3.21}$$

The receiving operator characteristic (ROC) curve shows the relation between the true positive rate and the false positive rate of a binary classifier depending on a parameter (threshold) range. The area under the ROC curve (AUC) evaluates the classifier performance across the range of thresholds. The AUC parameter is scale-invariant and threshold-invariant. AUC value ranges from 0 to 1, AUC close to 1 indicates good classifier performance, while AUC close to 0.5 denotes that the classifier performance is the same as of random classification.

Chapter 4

Results

This chapter presents the findings and results of completing the tasks in this thesis. Firstly, the analysed microelectrode recording (MER) data are specified in Section 4.1. Secondly, the subthalamic nucleus (STN) classification task is approached in Section 4.2 using thresholding and Support Vector Machine (SVM) classifiers. Thirdly, Section 4.3 maps beta activity along the exploration trajectory throughout STN. These findings are then compared to observations made in a broadband MER dataset of 1 bilateral DBS surgery in Section 4.4. Finally, beta activity extracted from clinical MER data is investigated in relation to severity of the cardinal PD symptoms (tremor, rigidity, and bradykinesia) in Section 4.5. In each task, the beta activity estimation methods listed in Section 3.3.4 were applied and their performance was compared. Such evaluation was however not trivial, as the ground truth for beta activity was missing in terms of both magnitude and localization.

4.1 Dataset

The subject of this thesis is exploration and analysis of an extensive clinical microelectrode recording (MER) dataset from deep brain stimulation (DBS) surgery of Parkinson's disease (PD) patients. Data were acquired and processed using the methods described in Chapter 3. The signals were band-pass filtered at 500-5000 Hz and sampled at 24 kHz upon recording with Medtronic LeadPoint system. Hereby utilized dataset was gathered at Na Homolce hospital, Prague, Czech republic, during the years 2008-2020. The latest surgery in our dataset was performed in July 2020. Only data from STN targeted DBS surgeries were used. The dataset contains microelectrode recordings from 298 DBS exploration measurements of 155 PD patients. Each exploration was measured with 5 electrodes in Ben-gun formation in multiple positions spaced in 0.5 mm increments of depth, as described Section 3.1. There were 47,490 recordings in the dataset. All signals were checked for artifacts using the maximum spectral difference method (MDP) prior to analysis, which caused shortening or discarding of recordings distorted by artifacts. Besides clinical signals, a broad band MER dataset was also acquired for 1 patient operated in 2020, which is used for exploration analysis in Section 4.4. The broadband MER recording setup was made by BrainScope. The signals are high-pass filtered at 10 Hz and sampled at 25 kHz. It was recorded with 5 microelectrodes at 9 positions in the left hemisphere and 8 positions in the right hemisphere, resulting in 85 recordings in total. The length of the broad band recordings varies from 30 s to 34 s.

4.2 Subthalamic nucleus classification from MER signals

The subthalamic nucleus (STN) was classified from MER signals using the normalized root mean square (NRMS) criterion and beta activity estimation methods described in Section 3.3.4. As stated in Section 2.4, classification of STN has been approached in the past and is well discussed in literature. The NRMS criterion introduced by [Moran et al., 2006] is now a gold standard in automatic STN localization. The purpose of this task is to determine whether the beta activity also changes dependently on the STN localization and whether it carries supplementary information to ameliorate the NRMS based classification. Additionally, it could be one of the possible ways to supply the missing ground truth for the beta activity and evaluate the performance of its estimation.

For the STN classification task, only trajectories, where the signals at the first 5 positions were available, were used. This selection was made to enable the normalization necessary for the NRMS criterion calculation. The final dataset used for classification consisted of data from 210 DBS surgeries from 128 patients composed of 14,593 microelectrode recordings in total. The signals from the first 5 positions were only used to calculate the reference signal power for normalization in NRMS. 13,544 remaining MERs were used for STN classification, out of which 4333 were labeled as inside STN and 9210 were outside STN. The dataset was randomly divided into training, validation, and testing data, which include 88, 20, and 20 patients, respectively. The training dataset included 140 explorations, containing 8948 MER signals, the validation dataset included 36 explorations, containing 2442 MER signals, and the testing dataset included 34 explorations, containing 2154 MER signals.

At first, the criteria were evaluated individually through thresholding classification on the training dataset. The corresponding ROC curves are plotted in Figure 4.1. Calculated areas under the curve (AUC) are recorded in Table 4.1. To consider varying thresholds in each exploration, the ROC and AUC measures were also evaluated for each criterion and exploration separately. The distribution of AUC values on the training dataset is shown in a boxplot in Figure 4.2.

criterion	AUC
NRMS	0.9369
rawMax beta	0.4007
envMax beta	0.7409
spikesOneMax beta	0.4538
spikesAllMax beta	0.4092
rawSum beta	0.3989
envSum beta	0.7401
spikesOneSum beta	0.4106
spikesAllSum beta	0.3614

Table 4.1: AUC for each method of STN classification on the training dataset.

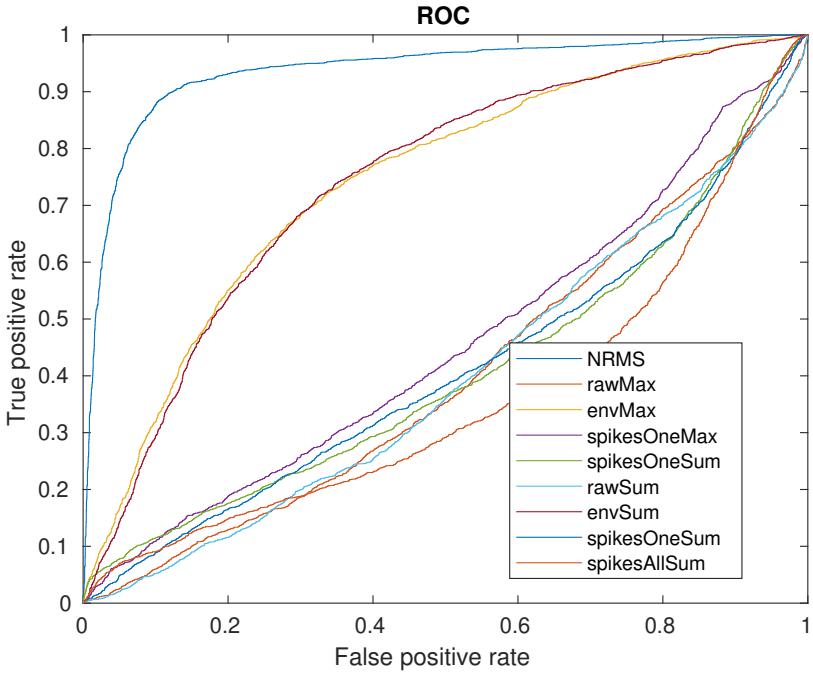

Figure 4.1: ROC for STN classifier based on NRMS and beta activity on the training dataset.

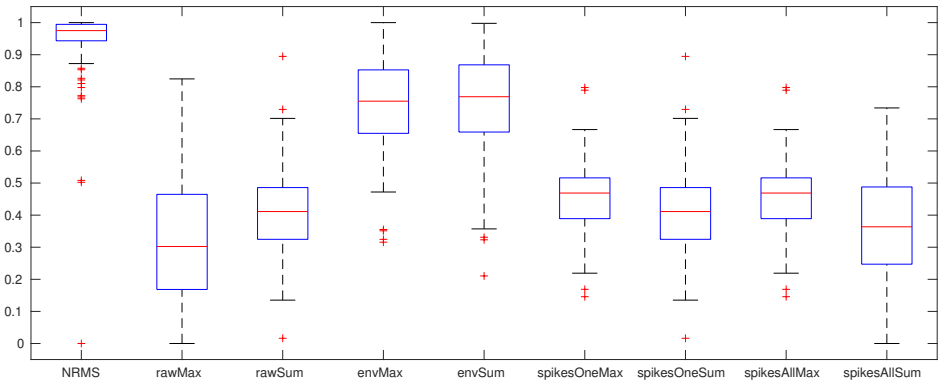

Figure 4.2: Distribution of AUC in testing dataset for each method of STN classification on the training dataset.

The NRMS criterion achieves the highest AUC value of 0.9369. As for the beta activity criteria, the *envMax* and *envSum* methods achieve the highest AUC values of 0.7409 and 0.7401, respectively. The AUC values for other types of beta activity are below 0.5. Such performance can be also explained by the correlation between the NRMS and the respective beta activity estimation method, which persists even after the signal normalization. A heatmap showing linear correlation between the evaluated criteria can be seen in Figure 4.3. Significantly high correlation between NRMS and methods based on signal envelope (*envMax, envSum*) explains higher classification performance of these methods compared to the other methods, where the AUC value is lower than 0.5. This observation is consistent with negative correlation between the NRMS and these criteria.

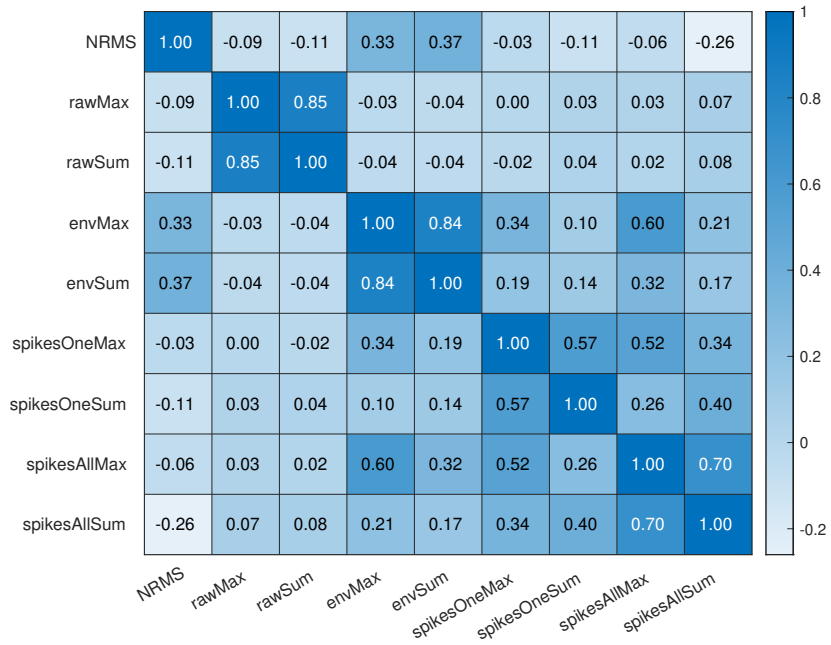

Figure 4.3: Correlation between all used STN classification criteria.

After the evaluation of individual criteria, a linear SVM was trained for combinations of the NRMS criterion with each beta activity estimation method. At first, 7 values of regularization constant C in the <0.001, 1000> range were tested. The linear SVMs were trained on the training dataset for each NRMS+beta combination and regularization constant value. The model performance was then evaluated on the validation dataset. The prediction accuracy ranged from 0.8526 to 0.8857, the sensitivity from 0.7129 to 0.7853, and the specificity from 0.9588 to 0.9723 on the validation dataset. The highest classification accuracy was seen for the C constant set to 0.1, 1, or 10 in all evaluated linear SVMs. To facilitate the comparison of beta activity estimation methods, we chose to set the regularization constant to 1 for further evaluation, which is a common choice. Results with scattered data and estimated class boundaries are shown in Figure 4.4.

The performance of the trained SVM classifiers on the testing dataset is recorded in Table 4.2. It can be observed that the estimated class boundary was independent on beta activity in all evaluated combinations. The resulting classifier depends almost exclusively on the NRMS feature. The optimal found threshold was $\theta = 2.0110$.

NRMS + beta	rawMax	envMax	spikesOneMax	spikesAllMax
Sensitivity	0.7908	0.0.7908	0.7908	0.7908
Specificity	0.9589	0.9589	0.9589	0.9589
Accuracy	0.9048	0.9048	0.9048	0.9048

NRMS + beta	rawSum	envSum	spikesOneSum	spikesAllSum
Sensitivity	0.7908	0.0.7908	0.7908	0.7908
Specificity	0.9589	0.9589	0.9589	0.9589
Accuracy	0.9048	0.9048	0.9048	0.9048

Table 4.2: Performance of the linear SVM on the testing dataset.

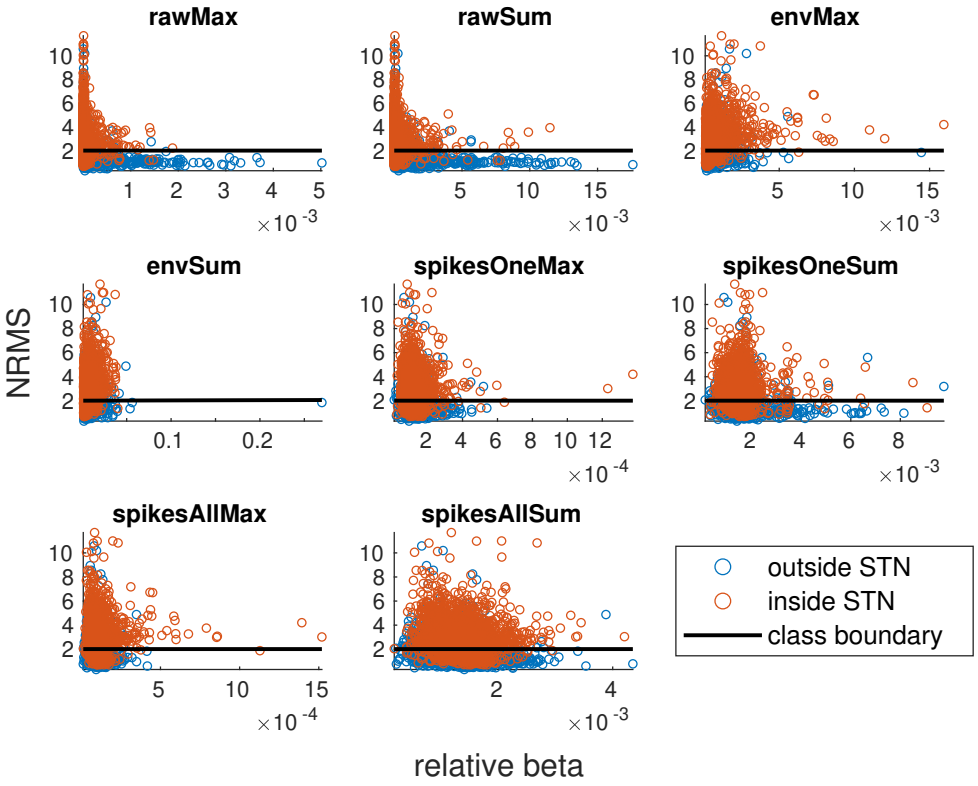

Figure 4.4: Results of STN classification on the training dataset using SVM.

Additionally, an SVM with Gaussian kernel was trained for the combinations of NRMS with each beta activity criterion. The results are recorded in Table 4.3.

NRMS + beta	rawMax	envMax	spikesOneMax	spikesAllMax
Sensitivity	0.8341	0.8341	0.8341	0.8326
Specificity	0.9459	0.9459	0.9459	0.9459
Accuracy	0.9099	0.9099	0.9099	0.9099

NRMS + beta	rawSum	envSum	spikesOneSum	spikesAllSum
Sensitivity	0.8341	0.8341	0.8341	0.8341
Specificity	0.9459	0.9459	0.9459	0.9459
Accuracy	0.9099	0.9099	0.9099	0.9099

Table 4.3: Performance of Gaussian kernel SVM on the testing dataset.

Changing the SVM kernel function from linear to Gaussian did slightly ameliorate the classifier performance on the testing dataset from 0.9048 to 0.9099. However, such small improvement may not outweigh the disadvantages of a complex model in the bias-variance trade-off. Besides, the linear model allows easy threshold adjustment according to the requirements on sensitivity and specificity. Therefore, the addition of beta activity did not improve classification of the whole STN. The extracted beta activity does not seem to reflect the activity of large neural populations, which are specific for STN. This is possibly due to the band-pass filtering of the clinical MER data.

4.3 Mapping beta activity in STN

During the DBS exploration, the electrodes are inserted into the brain from the anterio-dorso-lateral direction. The electrodes are in Ben-gun formation (as seen Figure 3.1). The motor subregion of STN is expected at the dorsolateral end as described by [Horn et al., 2017]. Therefore, posterior electrodes are more likely to insert this region than anterior electrodes. The intersection with the motor region is expected right at the beginning of STN labeled sector or shortly after entering the STN.

The beta activity was explored only in the positions labeled by surgeons as STN. Pairs of central-posterior and anterior-central electrodes were used to evaluate the differences in β activity at various distances from STN entry. Only explorations, where either a pair of central-posterior or anterior-central intersected with STN, were evaluated. In the central-posterior pair, the central electrode was considered the front electrode and the posterior electrode was considered the back electrode. In the anterior-central pair, the anterior electrode was considered the front electrode and the central electrode was considered the back electrode. In case all three electrodes (central, anterior, and posterior) intersected with STN, only the central-posterior pair was evaluated to maintain the explorations independency. In total, 3402 MER signals in 179 exploration electrode pairs were evaluated in this task.

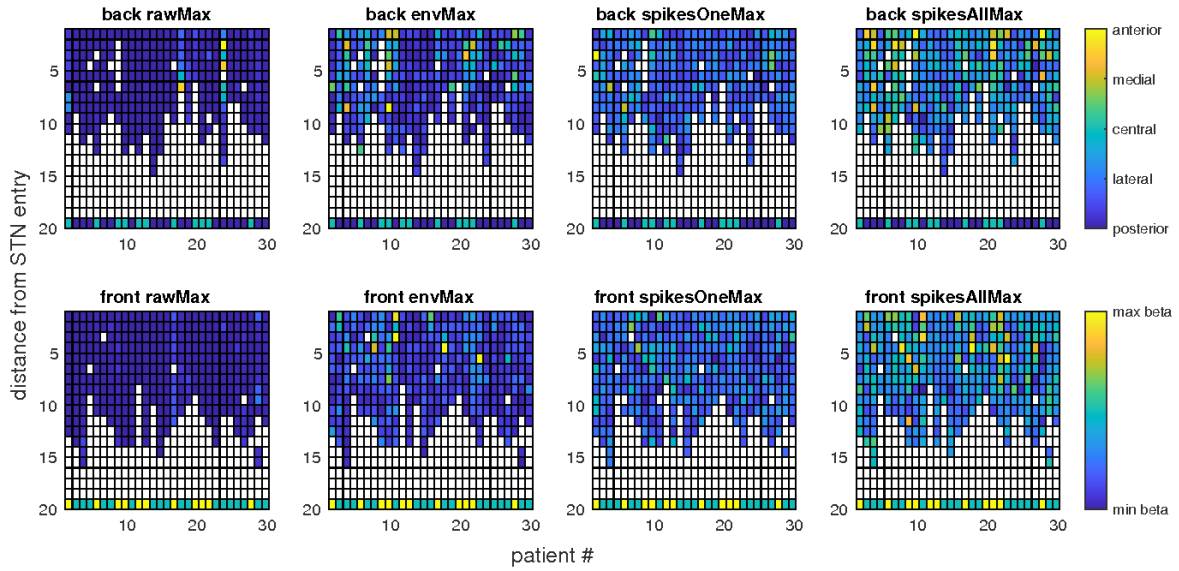

Figure 4.5: Visualization of the beta activity identified with *-Max* methods throughout the STN in a randomly selected subset of 30 patients for all estimation methods. The electrodes are color-coded at the bottom row of each graph. The legend to the color codes and beta activity magnitude is displayed on the right. The beta activity was scaled for illustration.

Higher beta activity was expected at the back electrode and at the beginning of STN. For illustration and rough visual comparison, the values of beta activity throughout the STN are displayed in paired heatmaps (upper and lower) for a randomly selected subset of 30 patients in Figures 4.5 and 4.6. There is a visible similarity between the heatmaps produced by *env* and *spikesAll* spectrum calculation methods, which agrees with their correlation seen in Figure 4.3. For these methods, a slightly higher beta activity can be seen at the beginning of the back electrode STN than in the front electrode, for example, in patients (columns) 3, 6,

9 20-22, 27, or 28, the first three rows indicate an elevated beta activity, which is not seen in their front counterpart. For the *raw* methods, a visibly increased beta activity at the back electrode can be seen in columns 17 or 23.

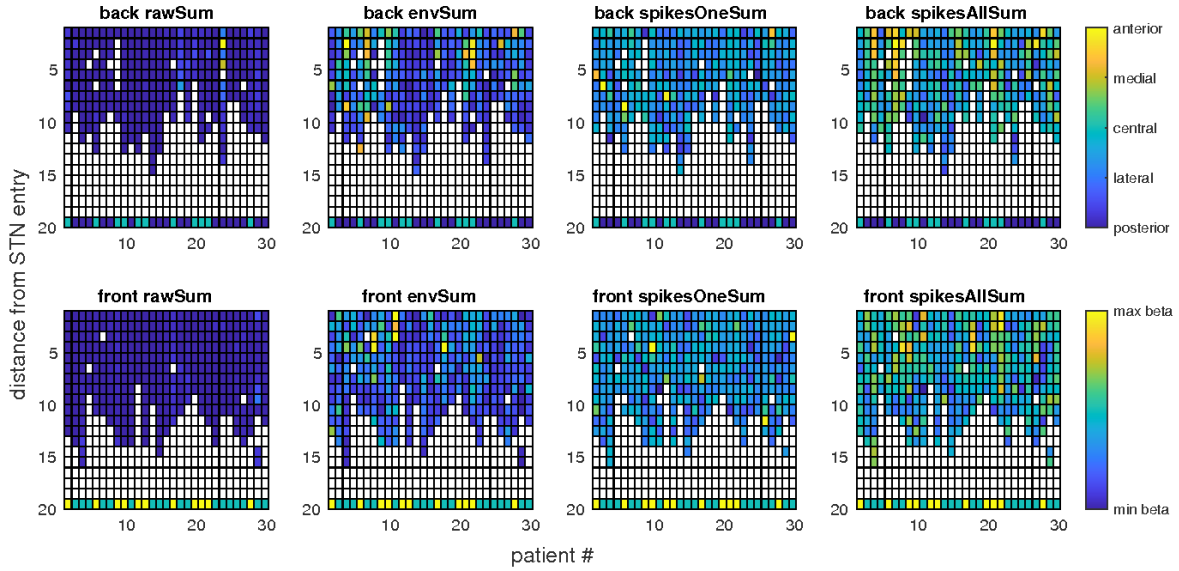

Figure 4.6: Visualization of the beta activity identified with *-Max* methods throughout the STN in a randomly selected subset of 30 patients for all estimation methods. The electrodes are color-coded at the bottom row of each graph. The legend to the color codes and beta activity magnitude is displayed on the right. The beta activity was scaled for illustration.

The differences between paired values at the back and front electrodes were evaluated at the corresponding positions (distances from entry to STN). The median value of beta activity at the back and front electrode throughout the positions is displayed in Figures 4.7 as well as the median difference between them, along with the 95% confidence intervals visualized as color bands around each median value. Finally, the paired differences were tested with Wilcoxon rank-sum test. The P-value of this test throughout the distances from STN entry for each method is plotted in Figure 4.8. The values of the paired tests correspond with the confidence intervals overlapping in Figure 4.7.

It can be observed that the *rawMax, spikesOneMax, rawSum*, and *spikesOneSum* methods result in highly overlapping confidence intervals in all positions, which also manifest as particularly high Wilcoxon rank-sum test P-values. The most significant results, i. e., the least overlapping confidence intervals and the lowest P-values in the first 2.0 mm of STN are present when the *envMax* method is used. The *envMax* beta activity is significantly higher at the back electrode than the front during the first five depth positions at the beginning of the STN. Beta activity generally decreases throughout the STN on both electrodes and the difference between them becomes smaller and less significant as the exploration proceeds in depth. These findings are in accord with the STN anatomy, expected motor subregion size, and typical trajectory direction. Therefore, *envMax* beta activity seems to be the most efficient in the motor subregion identification task. However, due to the lack of ground truth data (actual localization, final stimulation site, changes in response to medication), we cannot evaluate the objective performance.

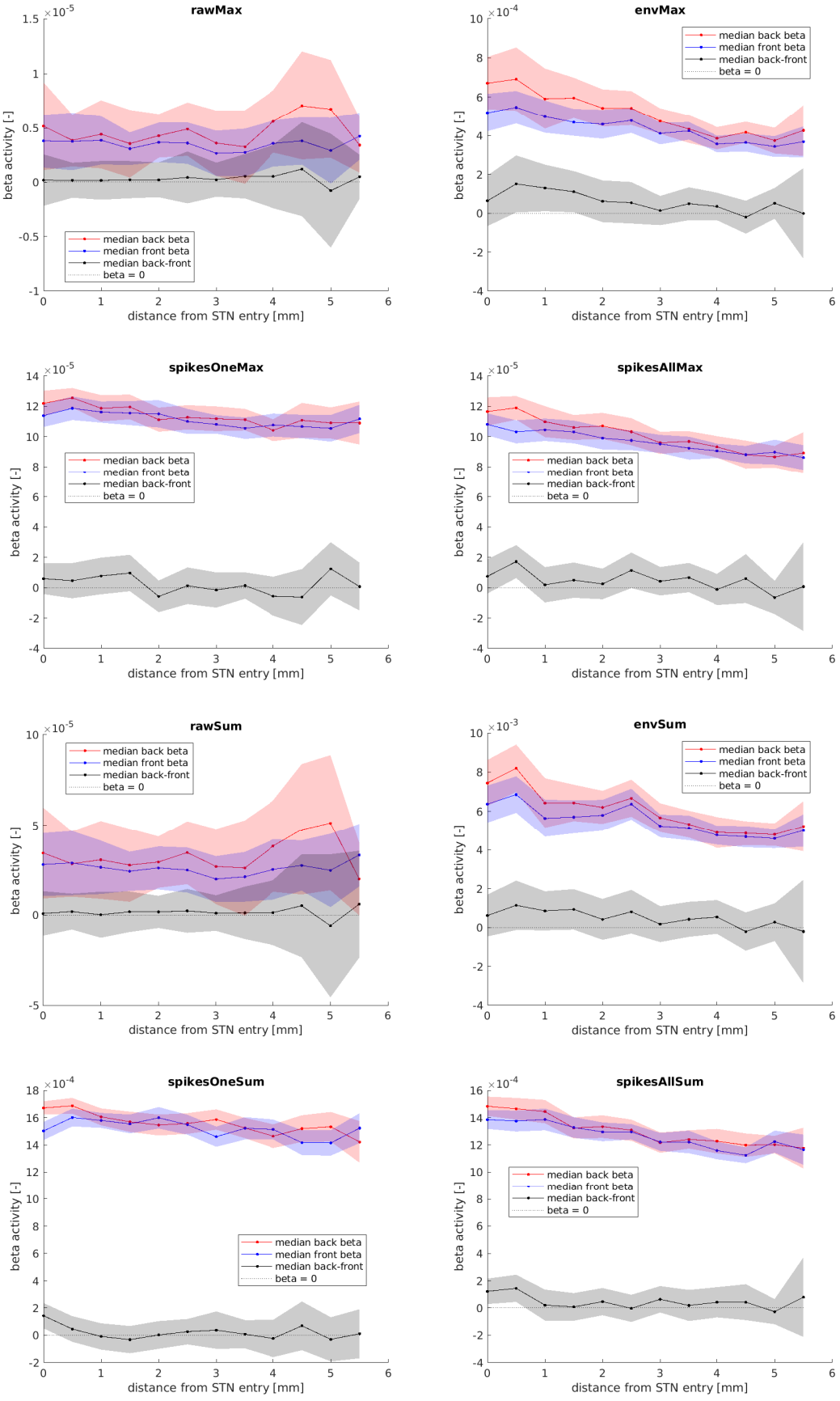

Figure 4.7: Median values and confidence intervals for all methods of beta activity estimation.

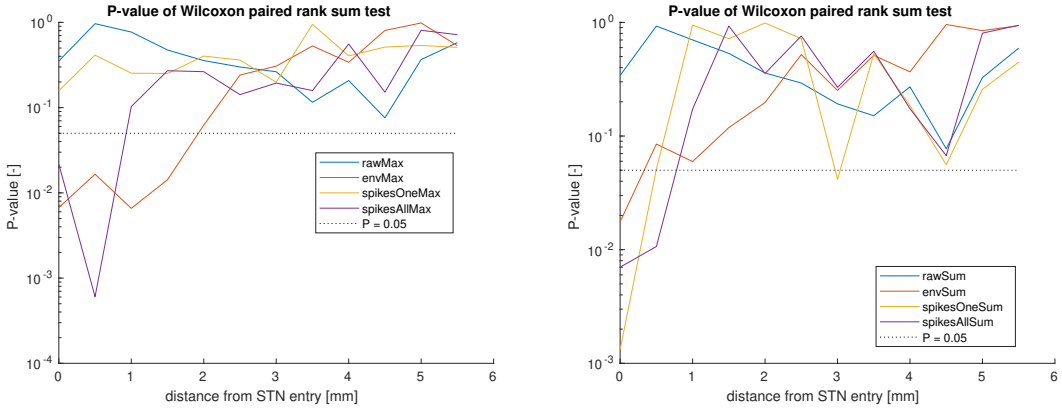

Figure 4.8: Wilcoxon rank-sum test for difference between beta activity on front and back electrode for the -*Max* methods (left) and -*Sum* methods (right)

4.4 Comparison of clinical and broadband MER

This section demonstrates the difference between the clinical MER and the nonfiltered broadband MER signals. The comparison is made with a dataset acquired from a bilateral DBS surgery on 1 patient, where the broadband MER was recorded simultaneously at the same set of 5 electrodes with the clinical MER, reflecting the basal activity. The broadband MER dataset is sampled at 25 kHz, high-pass filtered at 10 Hz, and is otherwise unlimited in frequency. It consists of synchronously recorded signals from all 5 electrodes in 9 positions in the left hemisphere (from T-6.5 to T-2.5) and 8 positions in the right hemisphere (from T-6.0 to T-2.5). The broadband dataset hence contains 85 recordings in total. The length of the recordings varies from 30 s to 34 s. To illustrate the difference between the clinical and broadband MER signal PSD, the spectrograms of the recordings are shown in Figures 4.9 and 4.11.

There are visible effects of the clinical recording band-pass filtering, especially in the STN positions, where the beta activity is less visible in the clinical MER than in the broadband MER. Such effects are also summed in the averaged PSD comparison in Figures 4.10 and 4.12. The beta band oscillatory activity is of similar values inside and outside the STN in the broadband data, while it is strongly mitigated inside the STN in the clinical MER data. The beta band PSD distribution of broadband data also differs from clinical data.

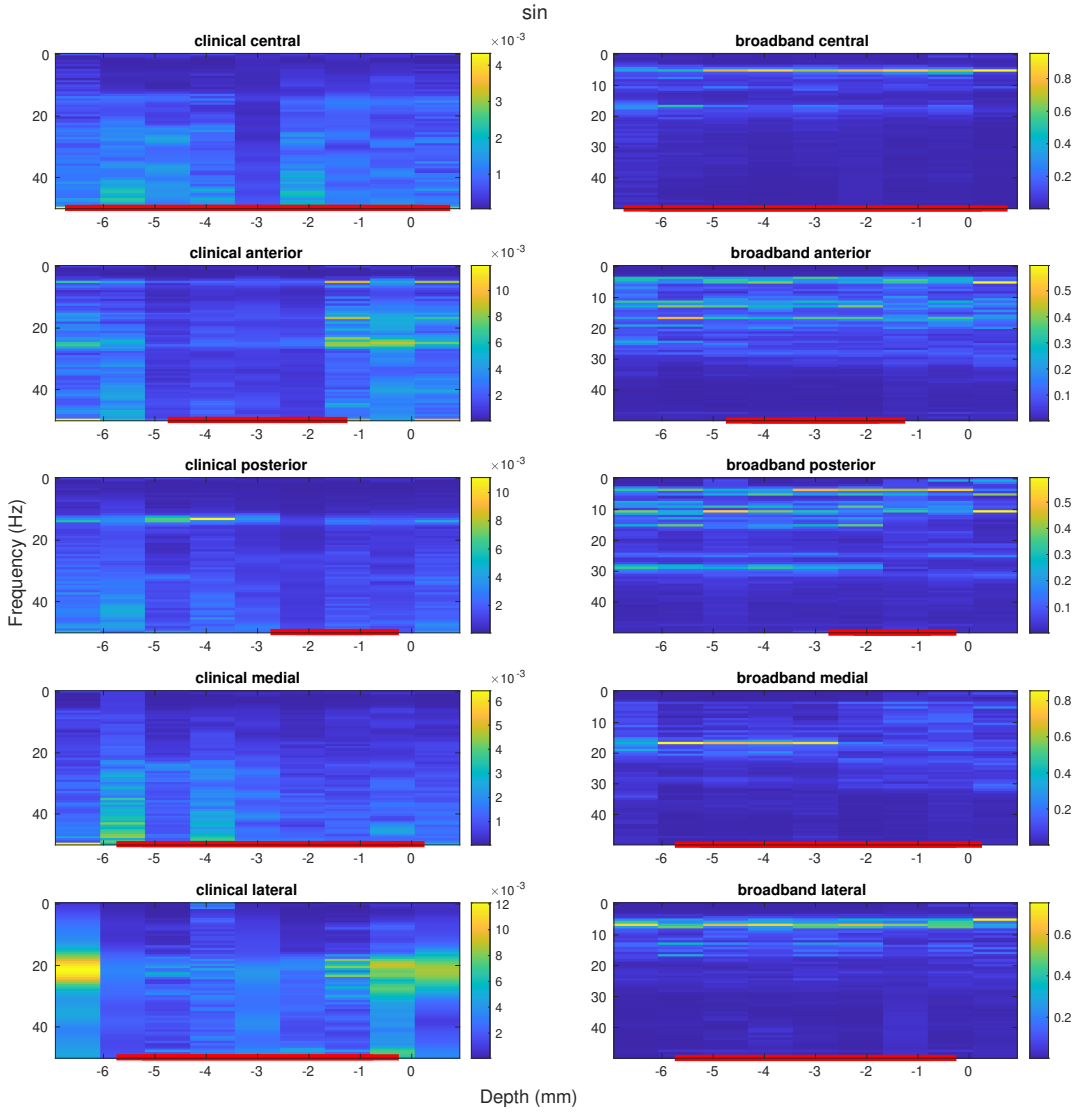

Figure 4.9: Spectrogram of the clinical microrecordings (left) and broadband microrecordings (right) on all electrodes and depths in range <T-6.5mm, T+0.5mm>. STN positions are marked with a red line on the bottom of the graph. Left hemisphere.

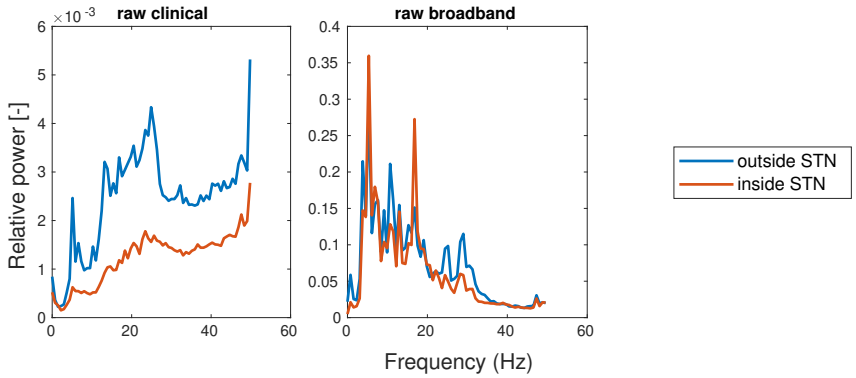

Figure 4.10: Averaged PSD of the clinical and broadband MER inside and outside the STN. Left hemisphere.

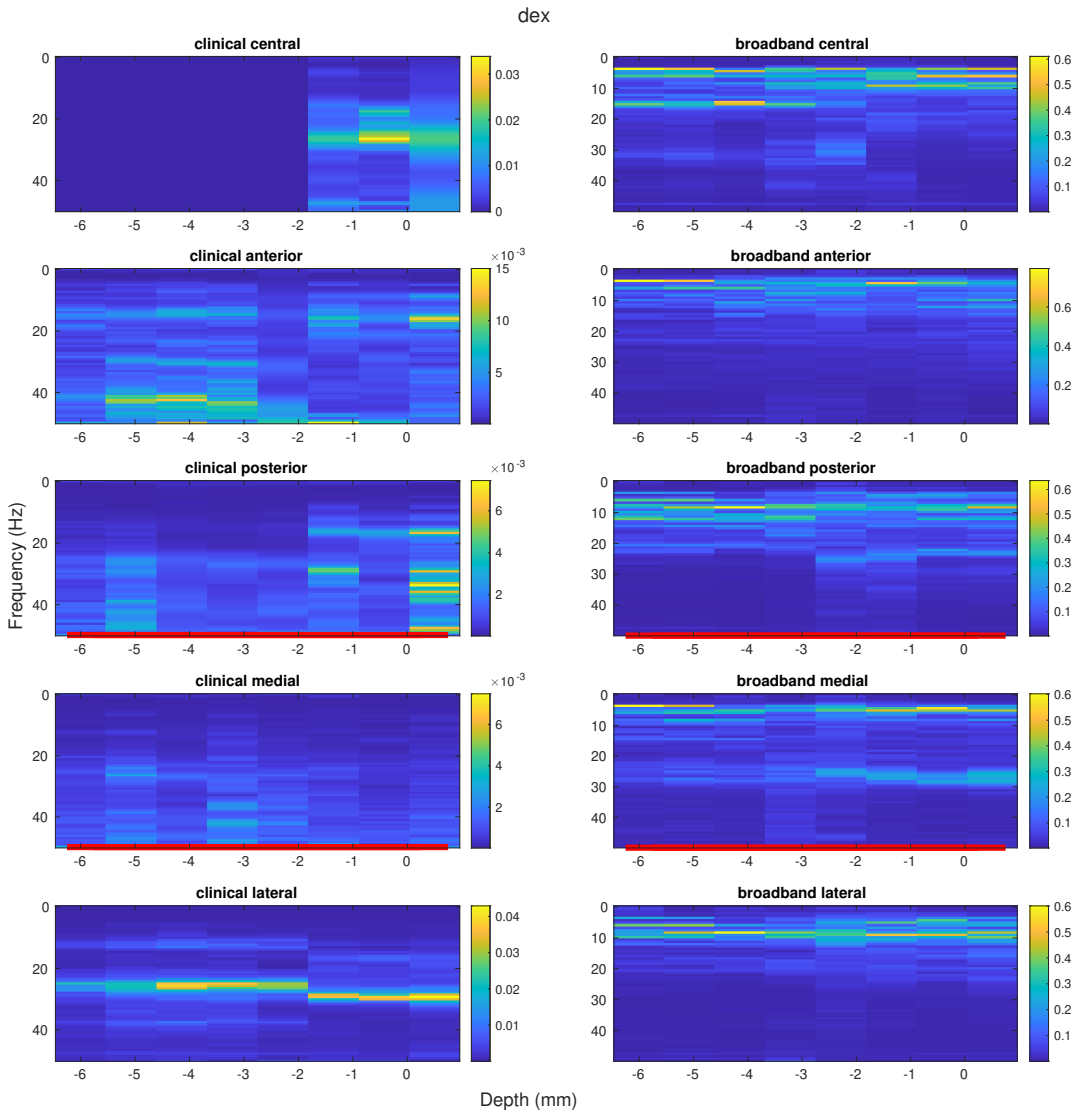

Figure 4.11: Spectrogram of the clinical microrecordings (left) and broadband microrecordings (right) on all electrodes and depths in range <T-6.0mm, T+0.5mm>. STN positions are marked with a red line on the bottom of the graph. Right hemisphere.

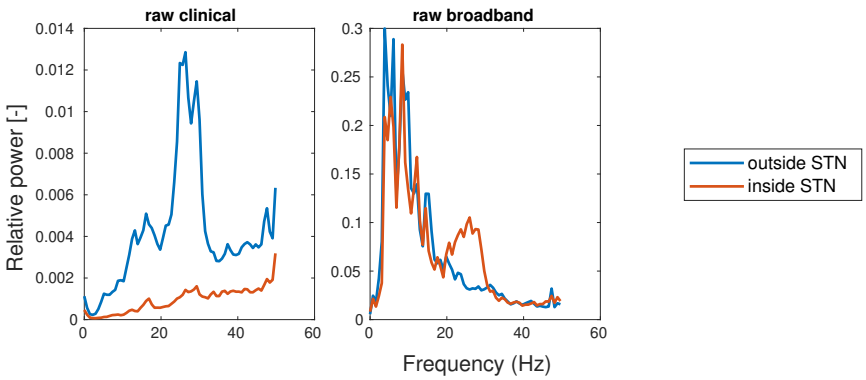

Figure 4.12: Averaged PSD of the clinical and broadband MER inside and outside the STN. Right hemisphere.

Additionally, the beta activity course throughout the STN was investigated using the broadband data and the clinical MER data as plotted in Figures 4.13 and 4.14. In the left hemisphere, there is a strongly pronounced oscillatory region in the broadband data, as seen in both Figures 4.9 and 4.13. Raw clinical data show a similar beta activity course in most electrodes. It is however shadowed by much stronger beta activity on the lateral electrode, which is not seen in the broadband data. The decreasing tendency of beta activity on the lateral electrode is partially reconstructed using spiketrain for PSD calculation (*spikesAllMax, spikesAllSum*). However, reconstructing the beta activity courses observed in other electrodes in the broadband MERs was not accomplished by any of the estimation methods applied to the clinical data. In the right hemisphere (Figure 4.14), the beta activity throughout STN is increasing in the broadband data, which differs from general expectations based on Section 4.3. Such tendency might be caused by the STN position and orientation alterations; e. g., due to the brain shift caused by previous implantation in the other hemisphere. Unfortunately, none of the estimations from clinical data reflects this observation in both posterior and medial electrodes.

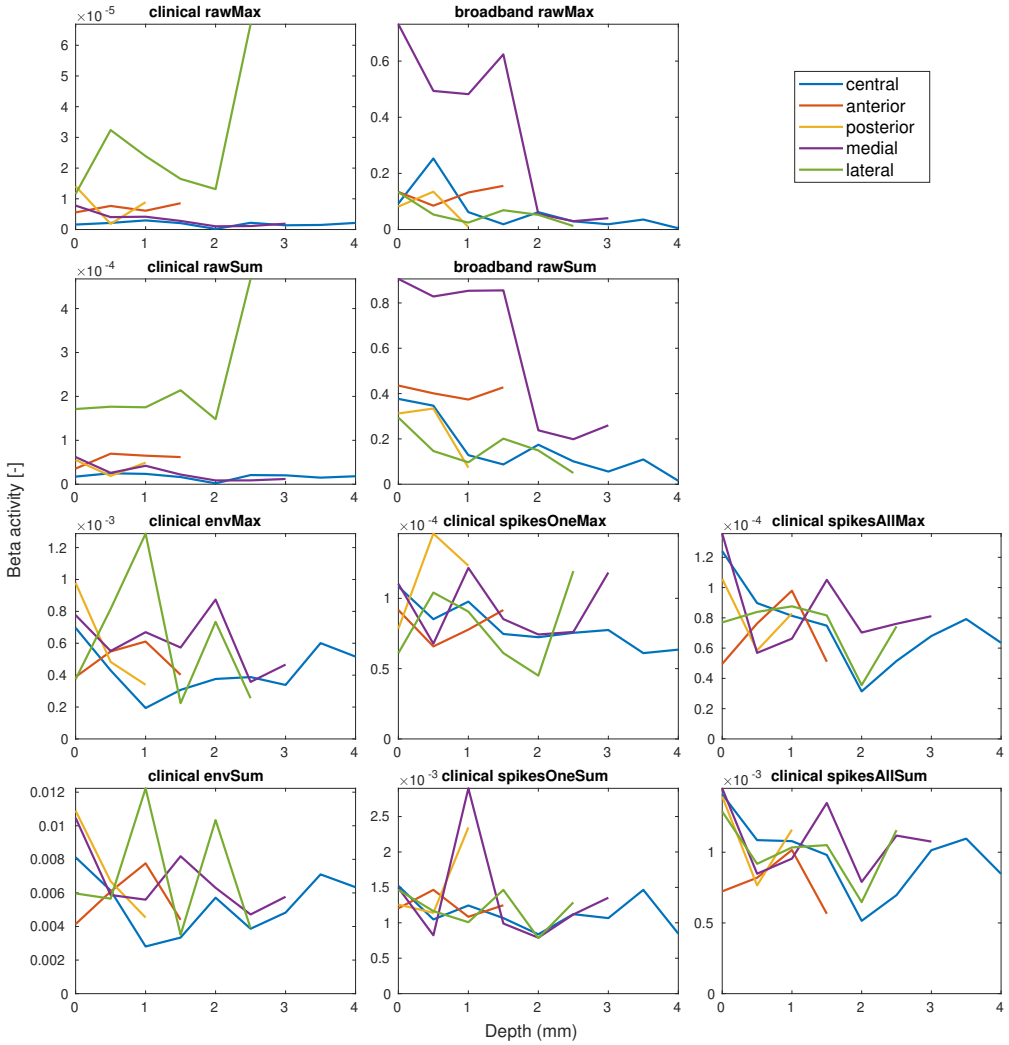

Figure 4.13: Beta activity course throughout the STN. Left hemisphere.

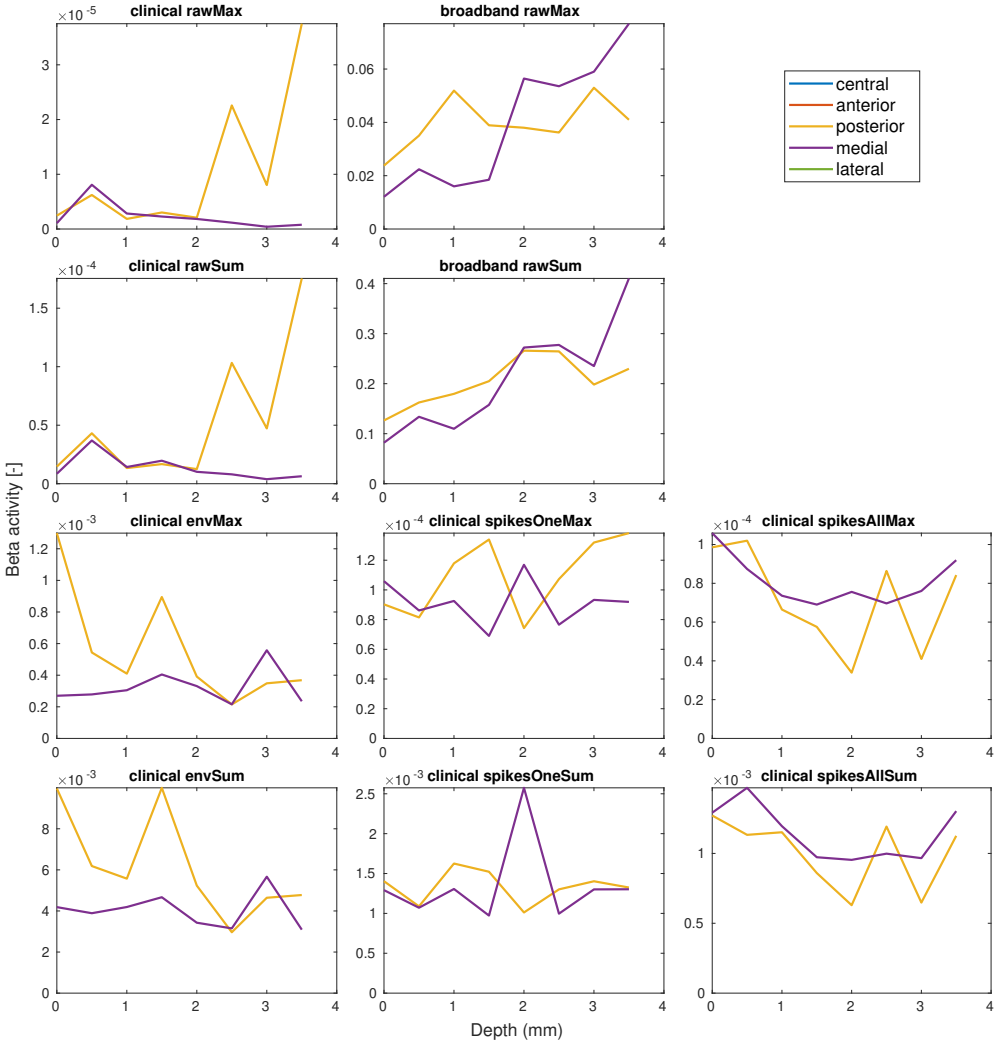

Figure 4.14: Beta activity course throughout the STN. Right hemisphere.

To quantitatively evaluate the comparison, the Pearson correlation between broadband and clinical MER beta activity was calculated on the dataset. The results are shown in Figure 4.15. None of the clinical beta activity was significantly correlated with the broadband beta activity. A borderline significant Pearson's correlation coefficient of 0.2848 and 0.2823 with P-values 0.0580 and 0.0602 was seen for *envSum* and *spikesAll* methods, respectively.

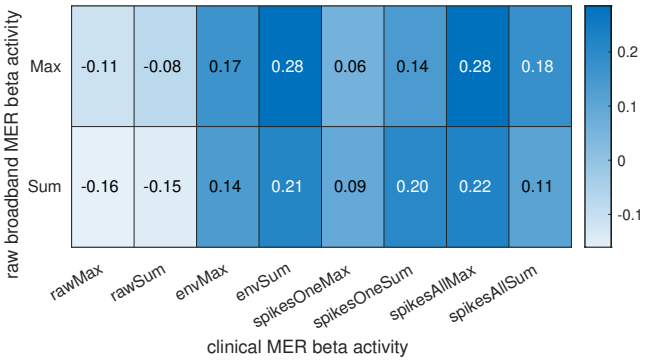

Figure 4.15: Correlation between the broadband and clinical MER beta activity.

4.5 Relation between beta activity and PD symptoms

To investigate the relation between the beta activity found in MER signals and the severity of PD symptoms, we have compared the extracted beta activity values and patients' UPDRS scores from the examination before the DBS surgery after an overnight medication withdrawal. For this task, we used data from 39 patients, out of which 16 patients underwent a bilateral surgery and 23 underwent a unilateral surgery. Therefore, the data come from 55 DBS surgeries in total, composing a dataset of 3591 microelectrode recordings. The evaluated symptoms were tremor, rigidity, and bradykinesia, which were investigated separately. Each symptom score is a sum of the corresponding ratings described in Section 2.7. The scores were calculated individually for each patient and side (left and right). Patient's overall beta activity was calculated using the methods described in Section 3.3.4 and averaged across the measured positions. According to literature, elevated beta activity and synchronization of neural populations (low frequency variance) observed inside the subthalamic nucleus indicates worse contralateral motor symptoms, especially rigidity. Thus, we expected the beta activity magnitude to be positively correlated with the symptom severity ratings. On the other hand, the variance of the peak beta frequency was expected to be negatively correlated with the symptom severity.

The Pearson correlation coefficients of the UPDRS tremor, rigidity and bradykinesia ratings and beta activity are displayed in Tables 4.4, 4.5 and 4.6. The mean beta activity value throughout the exploration is considered in Table 4.4 from all recorded positions and electrodes, while in Table 4.5 it is calculated from STN positions only. In Table 4.6, the variance of the frequency with maximum amplitude in the beta band (13-30 Hz) throughout the STN positions is compared against the UPDRS scores.

UPDRS score \ mean	rawMax	envMax	spikesOneMax	spikesAllMax
ipsilateral tremor	0.0411	-0.0415	-0.0816	-0.0225
contralateral tremor	-0.0261	0.0019	0.0575	0.1106
ipsilateral rigidity	***0.2939**	0.2031	0.2006	***0.3005**
contralateral rigidity	***0.3132**	-0.0185	***0.2790**	0.2232
ipsilateral bradykinesia	0.1591	0.1129	0.1973	0.1960
contralateral bradykinesia	0.1728	-0.0471	0.1405	0.0820

UPDRS score \ mean	rawSum	envSum	spikesOneSum	spikesAllSum
ipsilateral tremor	0.0561	-0.0557	-0.1639	-0.0382
contralateral tremor	0.0004	-0.0381	-0.0978	0.1625
ipsilateral rigidity	***0.3208**	0.1585	***0.2957**	****0.3707**
contralateral rigidity	***0.3165**	-0.0948	0.0647	0.2539
ipsilateral bradykinesia	0.1656	0.1187	0.0698	0.1483
contralateral bradykinesia	0.1702	-0.0259	0.0116	0.1048

Table 4.4: Pearson correlation coefficient between patients' UPDRS scores and mean beta activity value in all positions of an exploration. Values marked by * and ** are stastically significant with P-value <0.05 and <0.005 respectively .

UPDRS score \ mean	rawMax	envMax	spikesOneMax	spikesAllMax
ipsilateral tremor	-0.0082	-0.0180	-0.1383	-0.0788
contralateral tremor	0.0205	0.0271	0.0530	0.0683
ipsilateral rigidity	***0.3409**	0.2758	0.1833	***0.2819**
contralateral rigidity	0.1922	0.0853	0.2310	0.2196
ipsilateral bradykinesia	0.1174	0.1766	0.1784	0.1951
contralateral bradykinesia	0.0915	-0.0182	0.1156	0.0737

UPDRS score \ mean	rawSum	envSum	spikesOneSum	spikesAllSum
ipsilateral tremor	0.0092	0.0082	-0.1554	-0.0575
contralateral tremor	0.0361	0.0188	-0.0193	0.1761
ipsilateral rigidity	***0.3385**	***0.2857**	0.2004	***0.2822**
contralateral rigidity	0.2180	0.0544	0.0215	0.1623
ipsilateral bradykinesia	0.1156	0.1925	0.0065	0.1153
contralateral bradykinesia	0.0993	0.0091	-0.0816	0.0612

Table 4.5: Pearson correlation coefficient between patients' UPDRS scores and mean beta activity value in STN positions of an exploration. Values marked by * are stastically significant with P-value <0.05.

UPDRS score \ variance	rawMax	envMax	spikesOneMax	spikesAllMax
ipsilateral tremor	0.1732	-0.0203	-0.0805	-0.1734
contralateral tremor	* **0.3131**	-0.0354	0.1071	-0.0284
ipsilateral rigidity	-0.1508	0.1859	0.0778	-0.0667
contralateral rigidity	-0.2206	0.1536	0.1203	0.1746
ipsilateral bradykinesia	-0.0672	0.2715	0.0610	0.0820
contralateral bradykinesia	-0.0699	0.2092	0.0122	0.1822

Table 4.6: Pearson correlation coefficient between patients' UPDRS scores and variance of frequency with maximum amplitude in the beta band in STN positions of an exploration. Values marked by * are stastically significant with P-value <0.05.

A significant correlation between the rigidity UPDRS scores and mean beta activity measured from MER signals can be seen in Table 4.4. For beta activity estimated from raw signals, the coefficients are significant in all four cases (ipsilateral and contralateral rigidity vs. *rawMax* and *rawSum* methods). The ipsilateral rigidity score seems to be more significantly correlated with beta activity - it is significant for 5 beta activity estimation methods considering all recording positions and also for 5 methods when only STN positions are considered. Meanwhile, the contralateral rigidity only correlates with 3 methods of beta activity estimation. Furthermore, no significant correlations between contralateral rigidity and beta activity are observed if STN positions are considered only. As for the correlation between UPDRS scores and peak frequency variance in STN, the only significant correlation is between the contralateral tremor and the *rawMax* beta activity. However, due to the number of calculated correlations, this result could be also considered as false positive. If the significance level was adjusted with Bonferonni correction, none of the observed correlations would be significant. On the other hand, correlation significance in Tables 4.4 and 4.5 occured multiple times and consistently for rigidity scores, which supports the hypothesis of an existing correlation between the rigidity severity and beta activity.

Chapter 5

Discussion

This chapter comments the findings made in this thesis and discusses them in the context of existing research. We discuss the observations in the following order. Section 5.1 comments the implemented approaches to beta activity extraction from clinical MER data and potential relations between them. The subthalamic nucleus (STN) classification results are discussed in Section 5.2. Section 5.3 reviews the motor subregion identification inside the STN. Eventually, Section 5.5 evaluates the clinical relevance of the identified beta activity in relation to Parkinson's disease (PD) symptoms severity.

5.1 Beta activity identification

We have attempted to identify the beta activity (spectral activity in the 13 - 30 Hz frequency range) from the microelectrode recordings (MER) and use it for STN classification, the STN sensorimotor subregion, and its interpretation in relation to the clinical symptoms of Parkinson's disease. As the beta activity is not well defined in literature and the resources use different approaches [Zaidel et al., 2010], [van Wijk et al., 2017], [Horn et al., 2017], [Tinkhauser et al., 2018], [Milosevic et al., 2020], 8 methods of beta activity estimation were implemented and compared. They are based on 4 methods of signal extraction for PSD calculation (*raw, env, spikesOne*, *and spikesAll*) and 2 methods of beta activity interpretation from the normalized PSD (*Max* and *Sum*). In the heatmap of correlations between the criteria in Figure 4.3 is a visible relation between the -*Max* and -*Sum* methods calculated from the same PSD, which is an expected observation, as they are just different beta band interpretations of the same PSD. The correlation between the *spikesOne* and *spikesAll* methods is likely caused by a proportion of signals, where only one neural cluster was defined, hence the *spikesOne* and *spikesAll* PSD are the same. A surprisingly high correlation appears between the *env* methods and the normalized signal power (NRMS), which may be caused by relatively high beta band power compared to the rest of the envelope PSD. The envelope calculation in principle eliminates high frequencies, which increases the beta band power importance in the normalized PSD and causes seemingly higher relative beta activity in the STN positions, which are typically denoted by increased high frequency activity. Furthermore, the envelope methods highly correlate with the spiketrain methods, which is not caused by the remaining power in the beta band, as the correlation between the spiketrain methods and NRMS is negative. This observation can be explained as the envelope reflecting particularly high signal peaks recognized as spikes while mitigating signal fluctuations with

lower amplitudes. It also explains the higher correlation between the envelope and *spikesAll* methods than between the envelope and *spikesOne* methods, as the envelope does not perform any sort of spike sorting.

5.2 Subthalamic nucleus classification

The first discussed result is the subthalamic nucleus (STN) classification task. The criteria used for STN classification were the normalized root mean square (NRMS), which was also reviewed in literature as a reliable indication of STN [Moran et al., 2006]. Using the NRMS in combination with the implemented beta identification methods, 8 linear Support Vector Machines (SVM) were trained. The results displayed in Figure 4.4 are the same for all combinations. They show independence of STN classification on estimated beta activity. The resulting linear classifiers depend solely on the NRMS criterion and are therefore equivalent to a simple thresholding classification. Such findings are in accord with the evaluated single-criteria performance (see Table 4.1 and Figure 4.1) and their correlation (see Figure 4.3) as discussed in Section 5.1. The high precision of NRMS criterion was also expected as evaluated by [Konicarová, 2021]. An increased beta activity at the STN entry as seen in [Zaidel et al., 2010], [Horn et al., 2017],[van Wijk et al., 2017], [Koirala et al., 2020] and [Milosevic et al., 2020] was not observed. However, the main source of data in the cited literature are the local field potentials (LFP), which reflect the activity of neural populations and are not limited in low frequencies. Meanwhile, the signals in our dataset are band-pass filtered in 500 Hz - 5000 Hz upon recording, which is necessary for the audiovisual signal inspection and STN identification done by the surgeon. This also puts limitations on low-frequency activity, including the beta band. The acquired clinical MER signals thus rather reflect the spiking activity of nearby neurons than the synchronized neural populations activity at low frequencies. Therefore, the characteristics of the beta activity extracted from our data possibly differs from the LFP beta activity.

5.3 Motor subregion identification

After the classification of the subthalamic nucleus was evaluated, we have focused on identifying the motor subregion within. Multiple sources have reported the overlap between this area and the beta band oscillations. [Zaidel et al., 2010] identified a distinct dorsolateral oscillatory region, which is correlated with motor impairment severity and predicts on-stimulation medication response. [Milosevic et al., 2020] observed a statistically significant incidence between the maximum observed beta peak power and the final stimulation site using LFP physiology. Using the implemented extraction methods as listed in Section 3.3.4, we have mapped the beta activity course throughout the STN. Given the anterio-dorso-lateral direction of the exploration trajectory used at the clinical facility, which provided the data, we expected the highest beta activity in the first explored positions within the STN at the electrodes in the posterior part of the Ben-gun formation. Therefore, we have compared the beta activity at the anterior-central and central-posterior electrode pairs in the explorations, where they both penetrated the subthalamic nucleus. The results tested with Wilcoxon rank-sum (Mann-Whithney U) test are reported in Section 4.3. A significantly (P-value <0.05) higher beta activity was seen in the back electrode at the beginning of STN with *env* and *spikesAll* methods. The similar efficiency of the methods agrees with the correlation between them

as reported in Figure 4.3 and discussed above. The placement of the largest differences at the first 2.0 mm of STN is in accord with the expected position and size of the primary motor region as mapped by [Horn et al., 2017]. The decreasing significance in later STN positions possibly reflects varying length of the dorso-lateral oscillatory region as reported by [Zaidel et al., 2010]. From these findings, it seems that the *envMax* method, which had the most significant beta activity differences, efficiently mimics the beta activity extracted from LFP. However, this observation could not be verified with ground truth data as the information about the final stimulation placement and the medication response was missing.

5.4 Comparison to broadband MER data

The comparison of the clinical and broadband MER spectra shows that the band-pass filter affects the signal spectra critically. There was a striking difference between the mean broadband and clinical data power spectral density as seen in Figures 4.13 and 4.11. This difference affected the beta activity to a great extent as plotted in the beta activity course through STN in Figure 4.13 and 4.14, which are visually very different in the clinical and broadband data. As seen in the calculated Pearson correlation coefficients in Figure 4.15, none of the beta activity estimations from clinical data significantly correlated with the beta activity in the broadband data. The highest correlations, which were borderline significant were for the *envSum* and *spikesOneMax* methods. Surprisingly, the *envMax method*, which showed the highest performance in the STN mapping task in Section 4.3, does not show substantial correlation. While the inside and outside STN broadband spectra are similar in magnitude, in the case of the clinical data, they differ considerably as in the averaged PSD in Figures 4.10 and 4.14. The beta band power is suppressed more strongly in the inside STN recordings than outside STN. Such distortion may be caused by increased high-frequency activity inside STN leading to relatively lowered beta band importance in the normalized spectrum. Another cause of the difference may be an incidence with unknown regions outside the STN, which oscillate at beta frequencies. Such regions may include neural regulation pathways between the cortex and the basal ganglia as noted in [Michmizos et al., 2017]. These areas may also be potential candidates for deep brain stimulation, especially for patients who are not eligible for STN-DBS. For instance, deep brain stimulation of the caudal zona incerta, which is located close to the posterior tail of STN, has shown promising results reported by [Blomstedt et al., 2018].

5.5 Clinical interpretation of beta activity

At last, to provide a clinical interpretation of the extracted spectral features, the beta activity correlation with the Unified Parkinson's disease rating scale (UPDRS) scores for three cardinal Parkinson's disease symptoms (tremor, rigidity, and bradykinesia) was evaluated, which is reported in Section 4.5. Tremor and bradykinesia scores did not show any significant correlation with the investigated beta activity. A significant correlation was seen between the mean beta activity found during the whole DBS exploration and axial rigidity UPDRS scores. Contrary to the findings of [Tinkhauser et al., 2017], [Horn et al., 2017], and [Telkes et al., 2018], the contralateral rigidity did correlate with beta activity when all positions were considered, but not when they were limited to STN positions only. The high-frequency activity in STN may cause beta band suppression. Additionally, the beta activity observed outside the STN may

indicate neural synchronization at the beta frequency between the basal ganglia and cortical areas, which has been correlated to PD symptoms severity as reviewed by [Oswal et al., 2013] and [Chung et al., 2018]. On the other hand, the ipsilateral rigidity was significantly correlated with beta activity in both cases. This observation agrees with the findings of [Wild, 2015]. Other sources, such as [Horn et al., 2017], [Tinkhauser et al., 2017], and [Telkes et al., 2018], only report observations regarding the contralateral symptoms omitting the ipsilateral ones completely. The methods with the strongest and most consistent correlations were based on raw (artifact-filtered) MER signals and their unsorted spiketrains. As opposed to the expectations from previous tasks evaluation, the analytic envelope based methods did not perform so well. This suggest that different beta band characteristics may relate to the symptom severity than to the STN motor region identification. Given the number of evaluated correlation coefficients, a Bonferonni correction would be appropriate. Unfortunately, our findings are not strong enough to withstand such correction and they would all appear insignificant if the P-value threshold was adjusted. Nevertheless, the correlation significance appeared rather consistently for the same symptoms, which is unlikely in case of random occurrences. In addition to the mean beta activity, another hypothesis was made based on pathological neural synchronization at beta frequencies made by [Michmizos et al., 2017]. We observed the peak frequency variance in the beta band and its variance throughout the DBS exploration. However, there was only one significant correlation, which could be assumed as a random false positive occurrence given the high number of evaluations.

Chapter 6

Conclusion

This chapter concludes the achievements of individual tasks and the overall work in this thesis. Later, it mentions potential tasks for our future research on this topic. The assignment consisted of tasks listed as follows.

1. Study relevant literature on preprocessing of neuronal microelectrode recordings (MER) and their use for nuclei classification in deep brain stimulation (DBS) for Parkinson's disease (PD).
2. Prepare the dataset: convert and preprocess data from DBS surgeries including surgical protocols and other metadata.
3. Study, implement and evaluate methods for identification of the sensorimotor subregion of the subthalamic nucleus (STN) and identification of beta activity from MER signals. Compare your results on clinical data to non-filtered broadband MER data.
4. Implement a visualization tool for MER activity parameters in 3D.
5. Implement and evaluate an appropriate classifier for identification of the STN from MER signals. Evaluate performance of your classifier on the dataset from task 2.

Task 1 was answered with the resources listed in Bibliography at the end of this thesis. Among the literature, the essential titles were [Moran et al., 2006], [Zaidel et al., 2010] and [Bakštein, 2016], which are also listed in the assignment. There are publications from medical, electrical engineering, and computer science areas, as well as interdisciplinary ones. Given the broad scope of the topic and a long history (about three decades) of deep brain stimulation treatment in PD [Gardner, 2013], it is only a fraction of the available literature, which is most relevant to our work.

We have completed Task 2 prior to the remaining tasks. The data were acquired from the Na Homolce hospital, Prague, Czech Republic at the end of August 2020. The latest exploration processed in our dataset was performed in July 2020. After extracting the data from the hospital device, they were converted to .bin format and metadata (name, surgery date, hemisphere, and explored positions) were extracted and imported into our dbsProcessing Data Access Object framework developed by [Sieger, 2013]. Afterwards, the data were labeled according to the acquired operation protocol scans. The prepared dataset was later used for exploration and analysis in this thesis and is ready for exploitation in other tasks of our research group.

The results of Task 3 are reported in Sections 4.3 and 4.4. They are also discussed in Chapter 5. We were able to locate an increased beta oscillatory activity in the posterior part of detected STN with some of the implemented beta identification methods. However, given the lack of ground truth (actual sensorimotor region location, stimulation placement, medication response), it was not possible to verify our findings. In addition, the comparison to broadband data revealed critical differences from the clinical data. Unfortunately, only one bilateral DBS surgery in our dataset provided the broadband data as well. It was therefore not possible to make a more extensive comparison and deduce specific attributes of such differences.

The visualization tool assigned in Task 4 was implemented and used during the work for visual inspection and results verification in individual explorations. It can be either used as a MATLAB function or as a GUI application. Its function is briefly described in Section 3.4 and documented for potential users in Appendix A. The 3D exploration trajectory is represented by an electrode spacing in a Ben-gun formation. However, visualization of specific basal ganglia structures surrounding the electrodes was beyond the scope of this thesis. Besides the 3D tool, another tool was implemented to visualize the data and their spectral features in an operation protocol-like manner in a 2D grid plot. It was additionally employed in the 3D visualization GUI application and can be also used separately as a MATLAB function. It is described in Section 3.4 and documented in Appendix A. Both tools were implemented as part of our DAO framework and work as such.

The accomplishments of Task 5 are recorded in Section 4.2 and discussed in Chapter 5. We have implemented several criteria for STN classification based on the normalized root mean square (NRMS) and the beta activity extraction methods listed in 3.3.4. The normalized root mean square (NRMS) criterion reached a considerable 0.9048 precision on the testing dataset. This result agrees with findings made by [Moran et al., 2006], [Bakštein, 2016], and [Konicarová, 2021]. Contrary to expectations, when training linear SVM classifiers, beta activity was not found to be particularly helpful in STN classification. Changing the SVM kernel to Gaussian showed a slight improvement in the classifier performance. Such a small improvement (from 0.9048 precision to 0.9099) cannot uphold to the bias-variance trade-off of a complex model. As the resulting linear SVM classifier is equivalent to NRMS thresholding, it can be easily adjusted according to the requirements on sensitivity and specificity.

In addition to the assigned tasks, the relation of clinical MER beta activity to the PD symptoms severity was evaluated. The observations are reported in Section 4.5 and commented on in Chapter 5. Two of the inspected symptoms (tremor, bradykinesia) did not appear to be correlated with beta activity, while axial rigidity was significantly correlated with beta activity. As opposed to expectations, the correlations observed with the ipsilateral rigidity are more substantial than the contralateral rigidity. Nevertheless, such findings show a clinical relevance of the studied beta activity.

The hereby listed achievements could be elaborated on in our future research. For instance, adding new broadband MER data from recent DBS surgeries (since August 2020) would perhaps contribute to inside STN beta activity exploration. It would also reveal more attributes of clinical and broadband data comparison than the single surgery dataset we have attained. The implemented visualization tools are routinely used in visual signal inspection. The 3D beta activity visualization could be employed in atlas-fitting basal ganglia visualization developed by [Bakštein, 2016]. The atlas-fitting process could also provide additional information to the electrode localization, which would lead to a better understanding of the outside STN beta osillations observed in this thesis and their clinical relevance.

To conclude the thesis, we consider the assignment tasks to be fulfilled as requested. An extensive clinical microelectrode recording dataset was explored and analysed during our work. The main contributions were the dataset preparation, which is ready for use in further research, implemented visualization tools, which are routinely used for result verification through visual signal inspection. Besides facilitating the current work with data, we have devised new research questions concerning the beta oscillatory activity in clinical MER from STN-DBS surgery exploration. Although the results differ from expectations in some cases, they provide a meaningful insight to the beta activity interpretation in our data.

Bibliography

[Akram et al., 2017] Akram, H., Georgiev, D., Mahlknecht, P., Hyam, J., Foltynie, T., Limousin, P., Jahanshahi, M., Hariz, M., Zrinzo, L., Ashburner, J., Behrens, T., Sotiropoulos, S. N., Jbabdi, S., and De Vita, E. (2017). Subthalamic deep brain stimulation sweet spots and hyperdirect cortical connectivity in Parkinson's disease. *NeuroImage*, 158:332–345.

[Armstrong and Okun, 2020] Armstrong, M. J. and Okun, M. S. (2020). Diagnosis and Treatment of Parkinson Disease: A Review. *JAMA - Journal of the American Medical Association*, 323(6):548–560.

[Bakštein, 2016] Bakštein, E. (2016). *Deep Brain Recordings in Parkinson's Disease: Processing, Analysis and Fusion with Anatomical Models.* PhD thesis, Czech Technical University in Prague, Faculty of Electrical Engineering, Prague.

[Bakstein et al., 2016] Bakstein, E., Sieger, T., Novak, D., and Jech, R. (2016). Probabilistic model of neuronal background activity in deep brain stimulation trajectories. In *Lecture Notes in Computer Science (including subseries Lecture Notes in Artificial Intelligence and Lecture Notes in Bioinformatics)*, volume 9832 LNCS, pages 97–111. Springer Verlag.

[Bakštein et al., 2017] Bakštein, E., Sieger, T., Wild, J., Novák, D., Schneider, J., Vostatek, P., Urgošík, D., and Jech, R. (2017). Methods for automatic detection of artifacts in microelectrode recordings. *Journal of Neuroscience Methods*, 290:39–51.

[Bhidayasiri, 2005] Bhidayasiri, R. (2005). Differential diagnosis of common tremor syndromes. *Postgraduate Medical Journal*, 81(962):756–762.

[Blomstedt et al., 2018] Blomstedt, P., Persson, R. S., Hariz, G. M., Linder, J., Fredricks, A., Häggström, B., Philipsson, J., Forsgren, L., and Hariz, M. (2018). Deep brain stimulation in the caudal zona incerta versus best medical treatment in patients with Parkinson's disease: A randomised blinded evaluation. *Journal of Neurology, Neurosurgery and Psychiatry*, 89(7):710–716.

[Braak et al., 2003] Braak, H., Tredici, K. D., Rüb, U., De Vos, R. A. I., Jansen Steur, E. N. H., and Braak, E. (2003). Staging of brain pathology related to sporadic Parkinson's disease. *Neurobiology of Aging*, 24:191–211.

[Chaudhuri et al., 2010] Chaudhuri, K. R., Prieto-Jurcynska, C., Naidu, Y., Mitra, T., Frades-Payo, B., Tluk, S., Ruessmann, A., Odin, P., Macphee, G., Stocchi, F., Ondo, W., Sethi, K., Schapira, A. H., Castrillo, J. C. M., and Martinez-Martin, P. (2010). The nondeclaration of

nonmotor symptoms of Parkinson's disease to health care professionals: An international study using the nonmotor symptoms questionnaire. *Movement Disorders*, 25(6):704–709.

[Chou et al., 2018] Chou, K. L., Stacy, M., Simuni, T., Miyasaki, J., Oertel, W. H., Sethi, K., Fernandez, H. H., and Stocchi, F. (2018). The spectrum of "off" in Parkinson's disease: What have we learned over 40 years? *Parkinsonism and Related Disorders*, 51:9–16.

[Chung et al., 2018] Chung, J. W., Burciu, R. G., Ofori, E., Coombes, S. A., Christou, E. A., Okun, M. S., Hess, C. W., and Vaillancourt, D. E. (2018). Beta-band oscillations in the supplementary motor cortex are modulated by levodopa and associated with functional activity in the basal ganglia. *NeuroImage: Clinical*, 19:559–571.

[Contarino et al., 2012] Contarino, M. F., Bour, L. J., Bot, M., Van Den Munckhof, P., Speelman, J. D., Schuurman, P. R., and De Bie, R. M. (2012). Tremor-specific neuronal oscillation pattern in dorsal subthalamic nucleus of parkinsonian patients. *Brain Stimulation*, 5(3):305–314.

[Dallapiazza et al., 2018] Dallapiazza, R. F., De Vloo, P., Fomenko, A., Lee, D. J., Hamani, C., Munhoz, R. P., Hodale, M., Lozano, A. M., Fasano, A., and Kalia, S. K. (2018). *Parkinson's Disease: Pathogenesis and Clinical Aspects*. Codon Publications.

[Fox et al., 2018] Fox, S. H., Katzenschlager, R., Lim, S. Y., Barton, B., de Bie, R. M., Seppi, K., Coelho, M., and Sampaio, C. (2018). International Parkinson and movement disorder society evidence-based medicine review: Update on treatments for the motor symptoms of Parkinson's disease. *Movement Disorders*, 33(8):1248–1266.

[Gardner, 2013] Gardner, J. (2013). A history of deep brain stimulation: Technological innovation and the role of clinical assessment tools. *Social Studies of Science*, 43(5):707–728.

[Goetz et al., 2008] Goetz, C. G., Fahn, S., Martinez-Martin, P., Poewe, W., Sampaio, C., Stebbins, G. T., Stern, M. B., Tilley, B. C., Dodel, R., Dubois, B., Holloway, R., Jankovic, J., Kulisevsky, J., Lang, A. E., Lees, A., Leurgans, S., Lewitt, P. A., Nyenhuis, D., Olanow, W., Rascol, O., Schrag, A., Teresi, J. A., Van Hilten, J. J., and Lapelle, N. (2008). MDS-UPDRS. Technical report, International Movement Disorder Society, Milwaukee.

[Häusser, 2000] Häusser, M. (2000). The hodgkin-huxley theory of the action potential. *Nature Neuroscience*, 3(11s):1165.

[Heil, 2007] Heil, C. (2007). *Harmonic Analysis and Applications: In Honor of John J. Benedetto*. Applied and Numerical Harmonic Analysis. Birkhäuser Boston.

[Herrington et al., 2016] Herrington, T. M., Cheng, J. J., and Eskandar, E. N. (2016). Mechanisms of deep brain stimulation. *J Neurophysiol*, 115:19–38.

[Horn et al., 2017] Horn, A., Neumann, W. J., Degen, K., Schneider, G. H., and Kühn, A. A. (2017). Toward an electrophysiological "Sweet spot" for deep brain stimulation in the subthalamic nucleus. *Human Brain Mapping*, 38(7):3377–3390.

[Huebl et al., 2011] Huebl, J., Schoenecker, T., Siegert, S., Brücke, C., Schneider, G. H., Kupsch, A., Yarrow, K., and Kühn, A. A. (2011). Modulation of subthalamic alpha activity to emotional stimuli correlates with depressive symptoms in Parkinson's disease1. *Movement Disorders*, 26(3):477–483.

[Israel and Burchiel, 2004] Israel, Z. and Burchiel, K. J. (2004). *Microelectrode Recording in Movement Disorder Surgery*. Thieme, 1 edition.

[James et al., 2013] James, G., Witten, D., Hastie, T., and Tibshirani, R. (2013). *An Introduction to Statistical Learning with Applications in R*. Springer, New York, 7 edition.

[Koirala et al., 2020] Koirala, N., Serrano, L., Paschen, S., Falk, D., Anwar, A. R., Kuravi, P., Deuschl, G., Groppa, S., and Muthuraman, M. (2020). Mapping of subthalamic nucleus using microelectrode recordings during deep brain stimulation. *Scientific Reports*, 10(1).

[Konicarová, 2021] Konicarová, C.-A. (2021). *Klasifikace subthalamického jádra z mikroelektrodových záznamů*. PhD thesis, České vysoké učení technické, Fakulta elektrotechnická, Prague.

[Kringelbach et al., 2007] Kringelbach, M. L., Jenkinson, N., Owen, S. L., and Aziz, T. Z. (2007). Translational principles of deep brain stimulation. *Nature Reviews Neuroscience*, 8(8):623–635.

[Mathai and Smith, 2011] Mathai, A. and Smith, Y. (2011). The corticostriatal and corticosubthalamic pathways: Two entries, one target. So what? *Frontiers in Systems Neuroscience*, 5(64).

[Michmizos et al., 2017] Michmizos, K. P., Lindqvist, B., Wong, S., Hargreaves, E. L., Psychas, K., Mitsis, G. D., Danish, S. F., and Nikita, K. S. (2017). Computational Neuromodulation : Future Challenges for Deep Brain Stimulation [Life Sciences]. *IEEE Signal Processing Magazine*, 34(2):114–119.

[Milosevic et al., 2020] Milosevic, L., Scherer, M., Cebi, I., Guggenberger, R., Machetanz, K., Naros, G., Weiss, D., and Gharabaghi, A. (2020). Online Mapping With the Deep Brain Stimulation Lead: A Novel Targeting Tool in Parkinson's Disease. *Movement Disorders*, 35(9):1574–1586.

[Mohri et al., 2012] Mohri, M., Rostamizadeh, A., and Talwalkar, A. (2012). *Foundations of Machine Learning*. MIT Press, Cambridge.

[Moran et al., 2006] Moran, A., Bar-Gad, I., Bergman, H., and Israel, Z. (2006). Real-time refinement of subthalamic nucleus targeting using Bayesian decision-making on the root mean square measure. *Movement Disorders*, 21(9):1425–1431.

[Moustafa et al., 2016] Moustafa, A. A., Chakravarthy, S., Phillips, J. R., Gupta, A., Keri, S., Polner, B., Frank, M. J., and Jahanshahi, M. (2016). Motor symptoms in Parkinson's disease: A unified framework. *Neuroscience and Biobehavioral Reviews*, 68:727–740.

[Okun, 2012] Okun, M. S. (2012). Deep-Brain Stimulation for Parkinson's Disease. *New England Journal of Medicine*, 367(16):1529–1538.

[Oswal et al., 2013] Oswal, A., Brown, P., and Litvak, V. (2013). Synchronized neural oscillations and the pathophysiology of Parkinson's disease.

[Quian Quiroga and Nadasdy, 2004] Quian Quiroga, R. and Nadasdy, Z. (2004). Unsupervised Spike Detection and Sorting with Wavelets and Superparamagnetic Clustering. *Neural Computation*, 16:1661–1687.

[Rosin et al., 2011] Rosin, B., Slovik, M., Mitelman, R., Rivlin-Etzion, M., Haber, S. N., Israel, Z., Vaadia, E., and Bergman, H. (2011). Closed-loop deep brain stimulation is superior in ameliorating parkinsonism. *Neuron*, 72(2):370–384.

[Serranová et al., 2019] Serranová, T., Sieger, T., Růžička, F., Bakštein, E., Dušek, P., Vostatek, P., Novák, D., Růžička, E., Urgošík, D., and Jech, R. (2019). Topography of emotional valence and arousal within the motor part of the subthalamic nucleus in Parkinson's disease. *Scientific Reports*, 9(1).

[Sieger, 2013] Sieger, T. (2013). *Processing and Statistical Analysis of Single-Neuron Recordings*. PhD thesis, Czech Technical University in Prague, Faculty of Electrical Engineering, Prague.

[Silbernagl and Despopoulos, 2008] Silbernagl, S. and Despopoulos, A. (2008). *Color Atlas of Physiology*. Thieme, 6th edition.

[Telkes et al., 2018] Telkes, I., Viswanathan, A., Jimenez-Shahed, J., Abosch, A., Ozturk, M., Gupte, A., Jankovic, J., and Ince, N. F. (2018). Local field potentials of subthalamic nucleus contain electrophysiological footprints of motor subtypes of Parkinson's disease. *Proceedings of the National Academy of Sciences of the United States of America*, 115(36):E8567–E8576.

[Tinkhauser et al., 2017] Tinkhauser, G., Pogosyan, A., Tan, H., Herz, D. M., Kühn, A. A., and Brown, P. (2017). Beta burst dynamics in Parkinson's disease off and on dopaminergic medication. *Brain*, 140(11):2968–2981.

[Tinkhauser et al., 2018] Tinkhauser, G., Torrecillos, F., Duclos, Y., Tan, H., Pogosyan, A., Fischer, P., Carron, R., Welter, M. L., Karachi, C., Vandenberghe, W., Nuttin, B., Witjas, T., Régis, J., Azulay, J. P., Eusebio, A., and Brown, P. (2018). Beta burst coupling across the motor circuit in Parkinson's disease. *Neurobiology of Disease*, 117:217–225.

[van Wijk et al., 2017] van Wijk, B. C., Pogosyan, A., Hariz, M. I., Akram, H., Foltynie, T., Limousin, P., Horn, A., Ewert, S., Brown, P., and Litvak, V. (2017). Localization of beta and high-frequency oscillations within the subthalamic nucleus region. *NeuroImage: Clinical*, 16:175–183.

[Walckiers et al., 2010] Walckiers, G., Fuchs, B., Thiran, J. P., Mosig, J. R., and Pollo, C. (2010). Influence of the implanted pulse generator as reference electrode in finite element model of monopolar deep brain stimulation. *Journal of Neuroscience Methods*, 186(1):90–96.

[Welch, 1967] Welch, P. D. (1967). The Use of Fast Fourier Transform for the Estimation of Power Spectra: A Method Based on Time Averaging Over Short, Modified Periodograms. *IEEE Transactions on Audio and Electroacoustics*, 15(2):70–73.

[Wild, 2015] Wild, J. (2015). *Spike Sorting of Microelectrode Single-channel Recordings: Evaluation and Applications*. PhD thesis, Czech Technical University in Prague, Faculty of Electrical Engineering, Prague.

[Wild et al., 2012] Wild, J., Prekopcsak, Z., Sieger, T., Novak, D., and Jech, R. (2012). Performance comparison of extracellular spike sorting algorithms for single-channel recordings. *Journal of Neuroscience Methods*, 203(2):369–376.

[Zaidel et al., 2010] Zaidel, A., Spivak, A., Grieb, B., Bergman, H., and Israel, Z. (2010). Subthalamic span of β oscillations predicts deep brain stimulation efficacy for patients with Parkinson's disease. *Brain*, 133(7):2007–2021.

Appendix A

Visualization tools documentation

This appendix documents the software tools implemented within this thesis. The tools provide visualization of the microelectrode recoding (MER) signals acquired during deep brain stimulation (DBS) surgery and their spectral features. They are implemented in MATLAB and work as a part of our dbsProcessing Data Access Object (DAO) framework. It is therefore necessary to have the framework initialized prior to launching the visualization.

A.1 ProtocolPlot

The ProtocolPlot tool shows a MER dataset and respective power spectral density (PSD) in a structure similar to operation protocols. It has two parts: the grid plot and the close-up plot. In the grid plot, the recordings and their PSDs are plotted in a grid with STN positions denoted with a yellow background. When a position is clicked in the grid plot, a callback function plots the respective MER signal and the corresponding PSD in the close-up plot. The tool is implemented as a MATLAB function and works as a part of the dbsProcessing framework. It is therefore necessary to have the framework initialized. Besides other parts of dbsProcessing, the *calculateSpects* function must be also present in the framework. The function output variable is a handle to the created figure. The input parameters are listed as follows.

- patientID - exploration ID in DAO explorationPatients. Must be specified.
- spectMethod - signal feature type used for PSD calculation, which can be input as a single string (if only one PSD type is required) or a cell array of strings (a subset of available PSD methods); e. g., 'raw', 'env'. If not specified, the default parameter is 'raw'. Available methods are:
  - 'raw' - from raw (artifact-filtered) MER signals,
  - 'env' - from analytic envelopes of raw MER signals,
  - 'spikesOne' - from MER signal spiketrain - single cluster with the maximum amplitude,
  - 'spikesAll' - from MER signal spiketrain - including all clusters.
- minF - minimum frequency (in Hz) to be displayed, which also affects PSD scaling in the grid plot. If not specified, the default parameter is 3 Hz.

- maxF - maximum frequency (in Hz) to be displayed, which also affects PSD scaling in the grid plot. If not specified, the default parameter is 100 Hz.
- nfft - number of frequency bins (window length) for PSD calculation. The frequency resolution is equal to the sampling frequency divided by nfft. If not specified, the default parameter is 2^{15}.
- FS - sampling frequency (in Hz). If not specified, the default parameter is 24000 Hz.
- minBeta - minimum frequency (in Hz) of the range of interest; e. g., considered beta band. It is used for plotting the illustration vertical band borderlines in the grid plot. If not specified, the default parameter is 13 Hz. If not required, set the parameter value to NaN.
- maxBeta - maximum frequency (in Hz) of the range of interest; e. g., considered beta band. It is used for plotting the illustration vertical band borderlines in the grid plot. If not specified, the default parameter is 30 Hz. If not required, set the parameter value to NaN.
- filterMethod - artifact filtering method. It depends on the available methods in DAO; e. g., 'MDP' for maximum spectral difference method, 'cov' for covariance method, 'none' for no artifact filtering - assumes already filtered signals extracted from DAO or input in rawSignals. If not specified, the default parameter in 'none'.
- rawSignals - raw signals for plotting - must be of correct size (signal length, 5 electrodes, number of positions). If not specified, the signals are extracted from DAO according to patientID. If specified, the parameter overrides loading signals from DAO.
- spects - pre-calculated PSD in a cell array - each member is a matrix corresponding to the method specified in the spectMethod parameter. Must be of correct size (nfft, 5 electrodes, number of positions). If not specified, the spectra are calculated from the rawSignal input or recordings extracted from DAO. If specified, the input overrides PSD calculation.

The input and output parameter description can be also displayed in the command window by calling *help ProtocolPlot* command.

A.2 GUI-Beta3D

The GUI-Beta3D tool displays the spectral features of interest in Ben-gun electrode spacing in 3D. It was implemented using MATLAB AppDesigner. To run the application, the *dbs* struct of DAO framework must be initialized. Otherwise, the application will raise an error reported in the command line and terminate. The application can be launched by running *gui_beta3D* command or double-clicking the *gui_beta3D.mlapp* file in the file browser. The MER data are loaded and filtered for artifacts according to the current dbsProcessing settings.

A.2.1 Data selection

In the data selection control panels on the right of the application window, the user has the following choices. After setting the desired data selection parameters, the **Refresh Data** button on the right must be pressed to reload the MER signals and recalculate the respective PSD.

- Patient - the Patient dropdown menu shows a list of available exploration datasets, from which the desired exploration can be selected. The exploration codenames in the list are loaded from DAO.
- Spectrum method - the MER feature from which the power spectral densities should be calculated is selected through radio buttons in the Spectrum method panel. The parameter selected at the application launch is 'raw'.
  - raw - from raw MER signals,
  - env - from analytic envelopes of MER signals,
  - spikesOne - from MER signal spiketrain - single cluster with the maximum amplitude,
  - spikesAll - from MER signal spiketrain - including all clusters.
- Reference spectrum - the frequency range of interest is selected through the Reference spectrum panel. This range is also used for the PSD normalization. The frequencies are set in Hz. The minF must be set lower or equal to maxF, otherwise the plot will be cleared and an error message will be displayed instead The initial range of the reference spectrum is 3 Hz and 100 Hz for the minimum and maximum frequency, respectively.
  - min F - minimum frequency of the reference spectrum range.
  - max F - maximum frequency of the reference spectrum range.

A.2.2 Data visualization

The beta activity is visualized in a 3D plot in the application window. It is represented by five cylinders spaced in Ben-gun formation as during a DBS surgery. The vertical z axis represents the position depth, x and y axes represent the plane perpendicular to the exploration trajectory direction. The beta activity value is shown as diameter of the cylinder at each position. The values are scaled for better beta activity course illustration. For visualization of the currently calculated spectra, it is possible to select the beta band frequencies and the type of beta

activity representation in the Data visualization control panel at the bottom of the application window. After selecting such parameters, it is necessary to press **Refresh Plot** button to rewrite the current plot. It is however not necessary to press the **Refresh data** button if the parameters in the Data Selection panel remain the same.

- Beta band frequencies - In the minBeta and maxBeta sliders, the frequency range of expected beta activity can be selected. If minBeta is higher than maxBeta, or the Beta range is outside the Reference spectrum range, the plot will be cleared and an error message will be displayed instead. The initial values present at the application launch are 13 Hz and 30 Hz for the minimum and maximum frequency, respectively.
  - minBeta - the minimum frequency of the considered beta band.
  - maxBeta - the maximum frequency of the considered beta band.
- Beta activity type - on the right of the Data visualization control panel, there are options for beta activity type selection.
  - max - the plotted beta activity is the maximum power of one frequency bin in the selected beta band.
  - sum - the plotted beta activity is the summed power of the the whole selected beta band.

A.2.3 Protocol Plot

Each setting can be also visualized in a layout similar to operation protocols as when using the ProtocolPlot visualization tool. By clicking on the **Protocol Plot** button a new figure opens. The calculated spectra are plotted in a grid along with the original MERs from DAO. Positions annotated as STN are marked with yellow background. The plot is interactive, it can be moved and zoomed as usual MATLAB plots. Additionally, when clicking on a position area, the particular spectrum is plotted at the bottom left and the corresponding MER is plotted at the bottom right.

A.3 visualizeBeta3D

It is also possible to visualize the beta activity in a 3D electrode spacing without launching the GUI. The visualizeBeta3D tool creates the same plot as GUI-Beta3D, except the parameters cannot be adjusted interactively. It is implemented as a MATLAB function in the same manner as the ProtocolPlot tool and it also works as a part of our DAO framework. The output parameter is a handle to the created figure. The input parameters are listed as follows.

- patientID - exploration ID in DAO explorationPatients. Must be specified.
- spectMethod - signal feature type used for PSD calculation, which can be input as a single string (if only one PSD type is required) or a cell array of strings (a subset of available PSD methods); e. g., 'raw', 'env'. If not specified, the default parameter is 'raw'. Available methods are:

  - 'raw' - from raw (artifact-filtered) MER signals,
  - 'env' - from analytic envelopes of raw MER signals,
  - 'spikesOne' - from MER signal spiketrain - single cluster with the maximum amplitude,
  - 'spikesAll' - from MER signal spiketrain - including all clusters.
- minF - minimum frequency (in Hz) to be displayed, which also affects the PSD normalization. If not specified, the default parameter is 3 Hz.
- maxF - maximum frequency (in Hz) to be displayed, which also affects the PSD normalization. If not specified, the default parameter is 100 Hz.
- nfft - number of frequency bins. The frequency resolution is equal to the sampling frequency divided by nfft. If not specified, the default parameter is 2^{15}.
- FS - sampling frequency (in Hz) of the MER signal. If not specified, the default parameter is 24000 Hz.
- showMethod - the beta activity type to be plotted:
  - max - maximum power in beta band,
  - sum - summed power of the beta band.
- minBeta - minimum frequency (in Hz) of the range of interest; e. g., considered beta band. If not specified, the default parameter is 13 Hz.
- maxBeta - maximum frequency (in Hz) of the range of interest; e. g., considered beta band. If not specified, the default parameter is 30 Hz.
- spects - pre-calculated PSD in a cell array - each member is a matrix corresponding to the method specified in the spectMethod parameter. Must be of correct size (nfft, 5 electrodes, number of positions). If not specified, the spectra are calculated from the recordings extracted from DAO. If specified, the input overrides loading data from DAO and PSD calculation.

The input and output parameter description can be also displayed in the command window by calling *help visualizeBeta3D* command.

MASTER'S THESIS ASSIGNMENT

I. Personal and study details

Student's name: **Nguyenová Minh Thao** Personal ID number: **466018**

Faculty / Institute: **Faculty of Electrical Engineering**

Department / Institute: **Department of Computer Science**

Study program: **Medical Electronics and Bioinformatics**

Specialisation: **Bioinformatics**

II. Master's thesis details

Master's thesis title in English:

Analysis and classification of the subthalamic nucleus from microelectrode recordings

Master's thesis title in Czech:

Analýza a klasifikace subthalamického jádra z mikroelektrodových záznamů

Guidelines:

1. Study relevant literature on preprocessing of neuronal microelectrode recordings (MER) and their use for nuclei classification in deep brain stimulation (DBS) for Parkinson's disease (PD) [1-3]
2. Prepare the dataset: convert and preprocess data from DBS surgeries including surgical protocols and other metadata.
3. Study, implement and evaluate methods for identification of the sensorimotor subregion of the subthalamic nucleus (STN) and identification of beta activity from MER signals. Compare your results on clinical data to non-filtered broadband MER data.
4. Implement a visualization tool for MER activity parameters in 3D
5. Implement and evaluate an appropriate classifier for identification of the STN from MER signals. Evaluate performance of your classifier on the dataset from task 2.

Bibliography / sources:

[1] Moran, A., Bar-Gad, I., Bergman, H., & Israel, Z. (2006). Real-time refinement of subthalamic nucleus targeting using Bayesian decision-making on the root mean square measure. Mov Disord, 21(9), 1425–1431. https://doi.org/10.1002/mds.20995
[2] Zaidel, A., Spivak, A., Grieb, B., Bergman, H., & Israel, Z. (2010). Subthalamic span of β oscillations predicts deep brain stimulation efficacy for patients with Parkinson's disease. Brain, 133(7), 2007–2021. https://doi.org/10.1093/brain/awq144
[3] Bakštein, E. (2016) Deep Brain Recordings in Parkinson's Disease: Processing, Analysis and Fusion with Anatomical Models, doctoral thesis, Czech Technical Univeristy in Prague

Name and workplace of master's thesis supervisor:

Ing. Eduard Bakštein, Ph.D., Analysis and Interpretation of Biomedical Data, FEE

Name and workplace of second master's thesis supervisor or consultant:

Date of master's thesis assignment: **01.02.2021** Deadline for master's thesis submission: _____

Assignment valid until: **30.09.2022**

Ing. Eduard Bakštein, Ph.D. Supervisor's signature	Head of department's signature	prof. Mgr. Petr Páta, Ph.D. Dean's signature

III. Assignment receipt

The student acknowledges that the master's thesis is an individual work. The student must produce her thesis without the assistance of others, with the exception of provided consultations. Within the master's thesis, the author must state the names of consultants and include a list of references.

.	
Date of assignment receipt	Student's signature